

LAMELLAR INORGANIC SOLIDS AND BIOCHAR NANOCOMPOSITES FOR SORPTIVE
REMOVAL OF METAL IONS AND NITROPHENOL



A Thesis Submitted in Partial Fulfillment of the Requirements
for the Degree of Master of Science in Chemistry
Department of Chemistry
FACULTY OF SCIENCE
Chulalongkorn University
Academic Year 2021
Copyright of Chulalongkorn University

นาโนคอมพอลิตของของแข็งอินทรีย์แบบชั้นและถ่านชีวภาพสำหรับการจัดแบบดูดซับไอออนโลหะ
และไนโตรฟีนอล



วิทยานิพนธ์นี้เป็นส่วนหนึ่งของการศึกษาตามหลักสูตรปริญญาวิทยาศาสตรมหาบัณฑิต
สาขาวิชาเคมี ภาควิชาเคมี
คณะวิทยาศาสตร์ จุฬาลงกรณ์มหาวิทยาลัย
ปีการศึกษา 2564
ลิขสิทธิ์ของจุฬาลงกรณ์มหาวิทยาลัย

Thesis Title	LAMELLAR INORGANIC SOLIDS AND BIOCHAR NANOCOMPOSITES FOR SORPTIVE REMOVAL OF METAL IONS AND NITROPHENOL
By	Miss Sutasinee Sutthiklub
Field of Study	Chemistry
Thesis Advisor	Assistant Professor NIPAKA SUKPIROM, Ph.D.
Thesis Co Advisor	Associate Professor APICHAT IMYIM, Ph.D.

Accepted by the FACULTY OF SCIENCE, Chulalongkorn University in Partial
Fulfillment of the Requirement for the Master of Science

..... Dean of the FACULTY OF SCIENCE
(Professor POLKIT SANGVANICH, Ph.D.)

THESIS COMMITTEE

..... Chairman
(Professor VUDHICHAJ PARASUK, Ph.D.)

..... Thesis Advisor
(Assistant Professor NIPAKA SUKPIROM, Ph.D.)

..... Thesis Co-Advisor
(Associate Professor APICHAT IMYIM, Ph.D.)

..... Examiner
(Assistant Professor Wipark Anutrasakda, Ph.D.)

..... External Examiner
(Associate Professor Tosapol Maluangnont, Ph.D.)

สุธาลินี สุทธิกลับ : นาโนคอมพอลิตของของแข็งอนินทรีย์แบบชั้นและถ่านชีวภาพสำหรับการกำจัดแบบดูดซับไอออนโลหะและไนโตรฟีนอล. (LAMELLAR INORGANIC SOLIDS AND BIOCHAR NANOCOMPOSITES FOR ADSORPTIVE REMOVAL OF METAL IONS AND NITROPHENOL) อ.ที่ปรึกษาหลัก : ผศ. ดร.นันทกา สุขภิมย์, อ.ที่ปรึกษาร่วม : รศ. ดร.อภิชาติ อิมย์ม

งานวิจัยนี้ได้ทำการพัฒนาตัวดูดซับเป็นคอมพอลิตเพื่อขจัดสารพิษหลากหลายประเภท โดยให้ส่วนประกอบทั้ง 3 ส่วนเป็น เคลย์ แมกนีเซียม-อะลูมิเนียมเลเยอร์ดับเบิลไฮดรอกไซด์ (MgAl-LDH) และถ่านชีวภาพ เนื่องจากสารทั้งสามชนิดนี้เป็นตัวดูดซับที่ปลอดภัย มีราคาถูก และยังสามารถใช้ในการดูดซับและพื้นที่ผิวสูง คอมพอลิตจะถูกสังเคราะห์ด้วยวิธีโพล-ไพโรไลสิสร่วมกับการตกตะกอนร่วม และตรวจสอบลักษณะเฉพาะด้วยเทคนิค XRD และ SEM-EDS โดยพบว่าอนุภาคของเคลย์และ LDH กระจายตัวและผสมตัวอยู่บนเนื้อผิวของถ่านชีวภาพ ซึ่งเป็นการยืนยันการอยู่ร่วมกันของสามเฟสในระดับไมโครเมตรและนาโนเมตร

Ni^{2+} CrO_4^{2-} และ 4-ไนโตรฟีนอล เป็นตัวแทนสารเคมีปนเปื้อนชนิดแคตไอออน แอนไอออน และสารประกอบอินทรีย์สำหรับศึกษาการดูดซับในงานวิจัยนี้ โดยมีแบบจำลองการดูดซับทางจลนศาสตร์และแบบจำลองการดูดซับแบบไอโซเทอร์มใช้เพื่ออธิบายความจุและพฤติกรรมดูดซับของคอมพอลิตชนิดเคลย์/MgAl-LDH/ถ่านชีวภาพจากขานอ้อย (CLB) และ เคลย์/MgAl-LDH/ถ่านชีวภาพจากฟางข้าว (CLR) ซึ่งผลการดูดซับ Ni^{2+} เป็นไปตามแบบจำลองจลนศาสตร์อันดับสองเทียมและแบบจำลองไอโซเทอร์มของแลงเมียร์ โดยกลไกการดูดซับคาดว่าเกิดจากการแลกเปลี่ยนแคตไอออนระหว่าง Na^+ และ Ca^{2+} ในชั้นของเคลย์กับตัวดูดซับ Ni^{2+} ในขณะที่พฤติกรรมดูดซับของตัวดูดซับแอนไอออนของ CrO_4^{2-} ก็เข้ากันได้กับแบบจำลองจลนศาสตร์อันดับสองเทียมและแบบจำลองไอโซเทอร์มของแลงเมียร์ และกลไกการดูดซับที่เกิดขึ้นคือการแลกเปลี่ยน CrO_4^{2-} กับ NO_3^- และ OH^- ในชั้นของ MgAl-LDH ความสามารถในการดูดซับสูงสุด (Q_{max}) ของ CLB ต่อ Ni^{2+} และ CrO_4^{2-} คือ 13.2 mg g^{-1} และ 7.5 mg g^{-1} ตามลำดับ และของ CLR คือ 12.7 mg g^{-1} และ 6.1 mg g^{-1} ตามลำดับ สำหรับการดูดซับของ 4-ไนโตรฟีนอล สามารถอธิบายได้ด้วยแบบจำลองจลนศาสตร์อันดับสองเทียมและแบบจำลองไอโซเทอร์มของฟรุนลิช ซึ่งค่าความแรงของการดูดซับ (n) ของ CLB และ CLR คือ 1.7 และ 1.8 ตามลำดับ ซึ่งแสดงถึงการดูดซับที่ดี

นอกจากนี้การศึกษานี้ยังสำรวจเทคนิคการดูดซับแบบ fixed bed โดยใช้ตัวดูดซับ CLB และ CLR สำหรับขจัด 4-ไนโตรฟีนอล ประสิทธิภาพการดูดซับถูกนำเสนอโดยกราฟ breakthrough ซึ่งสอดคล้องกับอัตราส่วนของความเข้มข้นเริ่มต้นและความเข้มข้นคงเหลือและปริมาตรของ 4-ไนโตรฟีนอล ปริมาณการดูดซับสะสมของ CLB และ CLR คือ 0.88 mg g^{-1} และ 0.37 mg g^{-1} โดยชั้นตัวดูดซับมีความหนา 2 cm อัตราการไหล 0.3 mL min^{-1} และความเข้มข้นเริ่มต้น 10 mg L^{-1} งานวิจัยนี้แสดงให้เห็นว่าตัวดูดซับคอมพอลิตแบบสามส่วนเหล่านี้มีศักยภาพสูงในการเป็นตัวดูดซับสำหรับการกำจัดสารปนเปื้อนชนิดต่างๆ

สาขาวิชา เคมี
ปีการศึกษา 2564

ลายมือชื่อนิสิต
ลายมือชื่อ อ.ที่ปรึกษาหลัก
ลายมือชื่อ อ.ที่ปรึกษาร่วม

6172192423 : MAJOR CHEMISTRY

KEYWORD: Adsorption, Ternary composite adsorbent, Clay, Layered double hydroxide, Biochar

Sutasinee Sutthiklub : LAMELLAR INORGANIC SOLIDS AND BIOCHAR NANOCOMPOSITES FOR SORPTIVE REMOVAL OF METAL IONS AND NITROPHENOL. Advisor: Asst. Prof. NIPAKA SUKPIROM, Ph.D. Co-advisor: Assoc. Prof. APICHAT IMYIM, Ph.D.

In this research, the adsorbents of ternary-component composites were developed to remove various types of toxic chemicals. The selected three components are clay, MgAl-layered double hydroxide (MgAl-LDH) and biochar because they are nontoxic and low cost and also possess high adsorption capacity and high surface area. The composites were synthesized by the combination of post-pyrolysis and co-precipitation methods, and characterized by XRD and SEM-EDS. The result shows that clay and LDH particles distributed and deposited on the biochar matrix, confirming the coexistence of three phases in micrometer and nanometer scales.

Ni^{2+} , CrO_4^{2-} and 4-Nitrophenol were chosen as the representatives of chemical contaminant species of cation, anion, and organic compounds, respectively, for the adsorption study. The kinetic adsorption models and the isotherm adsorption models were used to explain the adsorption capacity and behavior of clay/MgAl-LDH/bagasse biochar composite (CLB) and clay/MgAl-LDH/rice straw biochar composite (CLR). The result of Ni^{2+} adsorption agreed with the pseudo-second-order kinetic model and the Langmuir isotherm model. The adsorption mechanism was proposed to be a cation exchange between Na^+ and Ca^{2+} in the interlayer of clay and the adsorbate Ni^{2+} . Meanwhile, the adsorption behavior of an anionic adsorbate CrO_4^{2-} was also well fitted with the pseudo-second-order kinetic model and the Langmuir isotherm model. The proposed adsorption mechanism was the exchange of CrO_4^{2-} with NO_3^- and CO_3^{2-} in the interlayer of MgAl-LDH. The maximum adsorption capacities (Q_{max}) of CLB were 13.2 mg g^{-1} and 7.5 mg g^{-1} towards Ni^{2+} and CrO_4^{2-} , respectively. Those of CLR were 12.7 mg g^{-1} and 6.1 mg g^{-1} , respectively. The adsorption of 4-Nitrophenol could be explained by the pseudo-second-order kinetic model and the Freundlich isotherm model. The adsorption intensity (n) of CLB and CLR were 1.7 and 1.8, respectively, indicating favorable adsorption.

In addition, this study explored the fixed bed adsorption technique by using the CLB and CLR for 4-nitrophenol removal. The adsorption performance was presented by the breakthrough curve corresponding to the ratio of the initial concentration, the residue concentration and the effluent volume of 4-nitrophenol. The cumulative adsorbed amounts of CLB and CLR were 0.88 mg g^{-1} and 0.37 mg g^{-1} , respectively, obtained using 2 cm bed thickness, 0.3 mL min^{-1} and the initial concentration of 10 mg L^{-1} . These ternary composite adsorbents were demonstrated as promising sorbents for the removal of various contaminant species.

Field of Study: Chemistry

Academic Year: 2021

Student's Signature

Advisor's Signature

Co-advisor's Signature

ACKNOWLEDGEMENTS

The author would like to express her sincere thanks to her thesis advisors, Assistant Professor Dr. Nipaka Sukpirom and Associate Professor Dr. Apichat Imyim, for their invaluable help and constant encouragement throughout this research. She would like to extend her appreciation to Professor Dr. Vudhichai Parasuk, Assistant Professor Dr. Wipark Anutrasakda, Dr. Junjuda Unruangsri, and Associate Professor Dr. Tosapol Maluangnont for their valuable suggestions.

In addition, she wishes to acknowledge all members of the Materials Chemistry and Catalysis Research Unit and Environmental Analysis Research Unit for their help and kind suggestion.

Finally, the author would like to express her deepest gratitude to her family and friends for their love, trust, support and kind suggestion throughout the period of this research.

Sutasinee Sutthiklub

TABLE OF CONTENTS

	Page
ABSTRACT (THAI).....	iii
ABSTRACT (ENGLISH).....	iv
ACKNOWLEDGEMENTS.....	v
TABLE OF CONTENTS.....	vi
LIST OF TABLES.....	vii
LIST OF FIGURES.....	viii
CHAPTER 1 INTRODUCTION.....	1
1.1 Background.....	1
1.2 Literature review.....	2
1.2.1 Adsorbents for the removal of pollutants in aqueous solution.....	2
1.2.1.1 Biochar.....	2
1.2.1.2 Clay.....	3
1.2.1.3 Layered Double Hydroxides.....	6
1.2.2 Biochar/based composites as adsorbents.....	7
1.2.2.1 Clay/biochar composites.....	8
1.2.2.2 LDH/biochar composites.....	10
1.3 Objectives.....	12
CHAPTER 2 EXPERIMENTAL.....	13
2.1 Raw materials.....	13
2.1.1 Biochar.....	13
2.1.2 Clay.....	13

2.2.1 Chemicals for MgAl-LDH.....	13
2.2 Chemicals.....	13
2.2.2 Chemicals for adsorbates.....	13
2.3 Preparation of clay/LDH/biochar composites	14
2.4 Characterizations	15
2.4.1 X-ray powder diffraction (XRD).....	15
2.4.2 Scanning Electron Microscopy (SEM)	15
2.4.3 Fourier Transform Infrared Spectroscopy (FTIR)	15
2.4.4 Surface area analysis.....	15
2.5 Adsorption experiments.....	15
2.5.1 Batch adsorption.....	16
2.5.1.1 Adsorption of Nickel(II)	16
2.5.1.2 Adsorption of Chromate anions	17
2.5.1.3 Adsorption of 4-nitrophenol	18
2.5.2 Fixed bed adsorption	18
CHAPTER 3 RESULTS AND DISCUSSION	20
3.1 Characterization of the composites	20
3.1.1 Structural and morphological analysis.....	20
3.1.2 Fourier Transform Infrared analysis (FTIR).....	23
3.1.3 Surface area and elemental analysis.....	25
3.2 Adsorption studies	27
3.2.1 Adsorption kinetics	27
3.2.2 Adsorption isotherms	32
3.2.3 Adsorption mechanism.....	39

3.3 Fixed bed adsorption	41
CHAPTER 4 CONCLUSIONS AND SUGGESTIONS	45
4.1 Conclusions	45
4.2 Suggestions for further research.....	46
REFERENCES	47
VITA.....	58



LIST OF TABLES

	Page
Table 3.1 FTIR absorbance bands and their assigned functional groups of the composites and pristine components.....	25
Table 3.2 Textural properties of the composites.....	26
Table 3.3 The adsorption kinetic parameters.....	28
Table 3.4 The adsorption isotherm parameters.....	33
Table 3.5 The comparison of Ni(II) adsorption capacity of the three-component composites with pristine components under given experimental conditions.....	38
Table 3.6 The comparison of CrO_4^{2-} adsorption capacity of the three-component composites with pristine components under given experimental conditions.....	38
Table 3.7 The comparison of 4-nitrophenol adsorption capacity of the three-components composites with pristine components under given experimental conditions.....	39
Table 3.8 The cumulative adsorbed amount of the composites.....	43

LIST OF FIGURES

	Page
Figure 1.1 Conceptual model identifying the adsorption mechanism of biochar [17]. .	3
Figure 1.2 Octahedral sheet.	4
Figure 1.3 Tetrahedral sheet.	4
Figure 1.4 Bentonite structure.....	5
Figure 1.5 The diagram of the adsorption mechanism of clay [22].	6
Figure 1.6 LDH Structure.	7
Figure 1.7 The diagram of the adsorption mechanism of LDH [25].	7
Figure 1.8 Diagrams of the post-pyrolysis and pre-pyrolysis procedures for the modification of biochar with LDH to create LDH/biochar composites.	10
Figure 2.1 Preparation of the composites.....	14
Figure 2.2 Batch adsorption.....	16
Figure 2.3 Colorimetric of Ni(II) complex with dimethylglyoxime.....	17
Figure 2.4 Fixed bed adsorption.....	18
Figure 2.5 Ideal breakthrough curve [49].	19
Figure 3.1 XRD patterns of CLB and CLR compared to the patterns of individual components.....	20
Figure 3.2 SEM images of individual components and the elemental mapping.....	21
Figure 3.3 SEM images of CLB and the elemental mapping.....	22
Figure 3.4 SEM images of CLR and the elemental mapping.....	23
Figure 3.5 FTIR spectra of the composites (CLB and CLR) and pristine components..	24
Figure 3.6 Adsorption/desorption isotherm of the composites.....	26
Figure 3.7 Adsorption kinetic data of Ni(II) ions.....	29
Figure 3.8 Adsorption kinetic data of CrO_4^{2-} anions.....	30

Figure 3.9 Adsorption kinetic data of 4-nitrophenol.	31
Figure 3.10 Adsorption isotherm data of Ni(II) ions.....	34
Figure 3.11 Adsorption isotherm data of CrO_4^{2-} anions.	35
Figure 3.12 Adsorption isotherm data of 4-nitrophenol.....	36
Figure 3.13 The schematic diagram of the adsorption mechanism.....	41
Figure 3.14 Breakthrough curve of 4-nitrophenol adsorption on CLB fixed bed column.....	42
Figure 3.15 Breakthrough curve of 4-nitrophenol adsorption on CLR fixed bed column.....	42



CHAPTER 1 INTRODUCTION

1.1 Background

Water pollutant is one of the most severe environmental problems. Organisms, plants, animals and humans have been affected by toxicity from contaminated water containing heavy metals, anionic pollutants and organic pollutants. Nickel(II) ion (Ni^{2+}) is one of the common toxic heavy metals pollutants [1], found in wastewaters from the industrial plants of stainless steel, nonferrous metal, coins, electroplating, and batteries [2][3]. A high concentration of Ni^{2+} can cause severe diseases in humans, such as skin dermatitis, rapid respiration, gastrointestinal disorder, lung cancer and bone cancer [4]. It can cause respiratory disease and abnormal liver function for aquatic animals [5]. In plants, it reduces the growth of shoot and root and lowers chlorophyll content [6]. The hexavalent chromium of chromate anion (CrO_4^{2-}) exists as a stable anionic species in water over a wide pH range. Cr(VI) is the most toxic form that is carcinogenic to living organisms. It induces liver damage, pulmonary congestion and causes ulcer formation [7]. 4-Nitrophenol is a toxic nitroaromatic pollutant and enters the environment during the production of drugs, pesticides and dyes [8]. It can damage the central nervous system, liver, kidney and blood of animals and humans [9].

These pollutants are difficult to degrade biologically and have high chemical toxicity; thus, they must be removed from wastewater before harming the aquatic

ecosystem. The adsorption process is one of the most popular separation techniques. Not only because its simplicity and cost-effectiveness, but also the adsorbates could remove toxic chemicals without causing any by-product. Therefore, the adsorption process has been widely used for the separation and purification system, especially water pollutant adsorption [10]. Many adsorbents such as clay, layered double hydroxide (LDH) and biochar are commonly used because they are low-cost, non-toxic, and eco-friendly. Some of them have high surface area, leading to high adsorption capacity; therefore, they were selected in this work.

1.2 Literature review

1.2.1 Adsorbents for the removal of pollutants in aqueous solution

1.2.1.1 Biochar

Biochar is carbonaceous porous materials derived from carbon-rich agriculture crop residues under slow pyrolysis; hence, it is known and widely used as low-cost and environmentally friendly adsorbents. The physicochemical properties that influence the adsorption behavior include high surface area and high porosity, high surface charge density. And its surface could bear some functional groups. Therefore, it was reported as the adsorbents for various pollutants such as dyes [11], heavy metals (e.g. Cu(II) [12], Hg(II) [13], Zn(II) and Ni(II) [14]), phosphate [15] and nitrate [16] in aqueous solution. Surface functionality affects to biochar adsorption mechanism by ionic exchange, electrostatic attraction and surface precipitation (Figure 1.1).

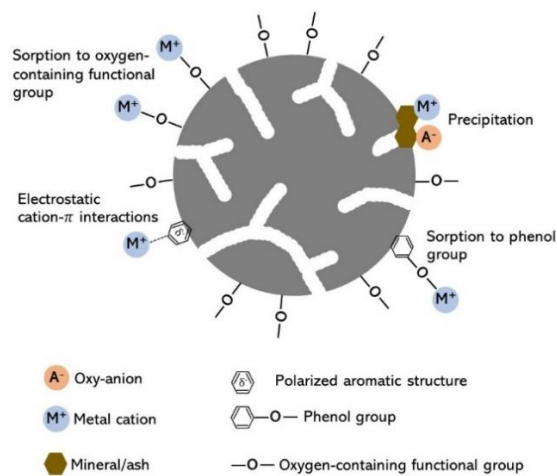


Figure 1.1 Conceptual model identifying the adsorption mechanism of biochar [17].

1.2.1.2 Clay

Clay minerals is the term of hydrous layered silicates group or phyllosilicates group. Each layered structure of clays is the combination of two layered structure units, including octahedral and tetrahedral layers. The octahedral layer consists of two parallel, closely packed planes of six oxygen (O) atoms or hydroxyl groups (OH⁻) at the corner and a cation in the center. Aluminum (Al), magnesium (Mg) and iron (Fe) ions are usually the centered cation in an octahedral sheet (Figure 1.2). Another structure unit, the tetrahedral layer is composed of a silicon (Si) atom surrounded by four oxygen (O) atoms or hydroxyl groups (OH⁻) in a tetrahedral sheet. The silicon tetrahedron combines with several silicon tetrahedra by edge-linking with oxygen or hydroxyl to make a hexagonal network (Figure 1.3). The assemblage of these layers can classify the type of clay minerals groups, for instance, smectite, micas, kaolinite, chlorite and sepiolite, etc. [18]

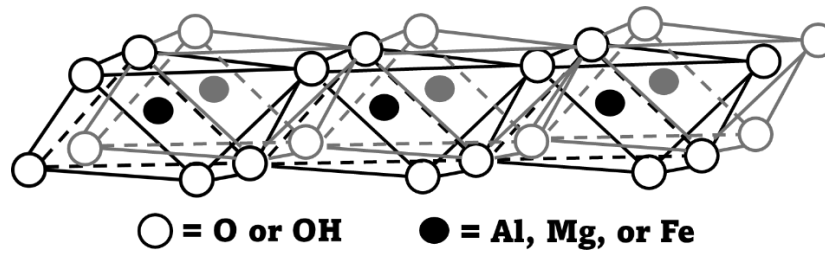


Figure 1.2 Octahedral sheet.

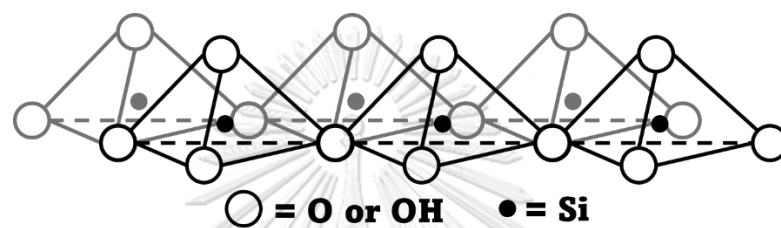


Figure 1.3 Tetrahedral sheet.

Bentonite is one of the minerals in the smectite clay mineral group, which occurs from volcanic ash or tuff in the marine environment, and consists mostly of montmorillonite. The idealized chemical formula is $A_x(\text{Al}_{4-x}\text{Mg}_x)\text{Si}_8\text{O}_{20}(\text{OH})_4 \cdot n\text{H}_2\text{O}$ (where A is a monovalent or divalent cation presenting in the interlayer of clay structure) for the montmorillonite, A is normally Na^+ , K^+ , and Ca^{2+} . The characteristic structure layer is a 2:1 layer, as shown in Figure 1.4, comprising of two silicon-centered tetrahedral sheets articulated to one aluminum-centered octahedral sheet. Its layer is negatively charged and gets neutralized by cations (A) within the interlayer. This type of clay has attractive properties such as relatively high surface area, high ion exchange capacity and low-cost [19]. Therefore, they have been

commonly used as adsorbents to remove various pollutants such as heavy metal ions (e.g., Co^{2+} , Cu^{2+} , Ni^{2+} , Pb^{2+} , Zn^{2+} , Cr^{6+} and Cd^{2+}) [20] and organic compounds (e.g., phenol, benzene and 4-nitrophenol) [21]. Montmorillonite displays the adsorption mechanism through cation exchange in the interlayer, ligand exchange and surface precipitation with OH^- on the tetrahedral sheet (Figure 1.5).

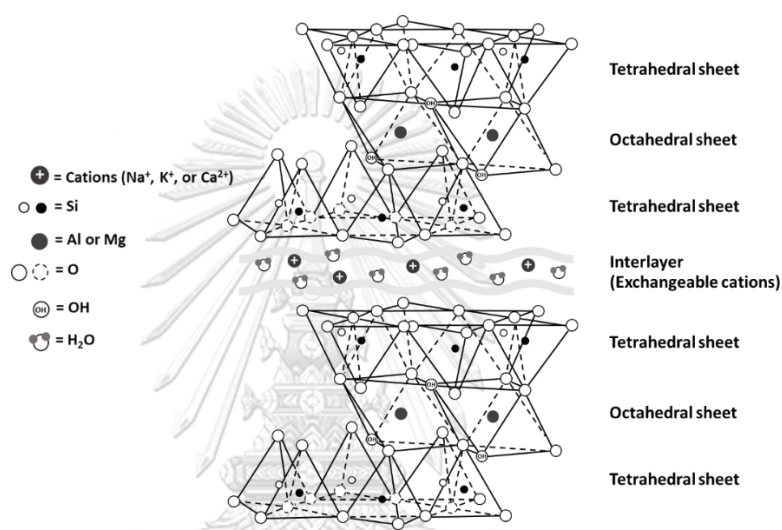


Figure 1.4 Bentonite structure.

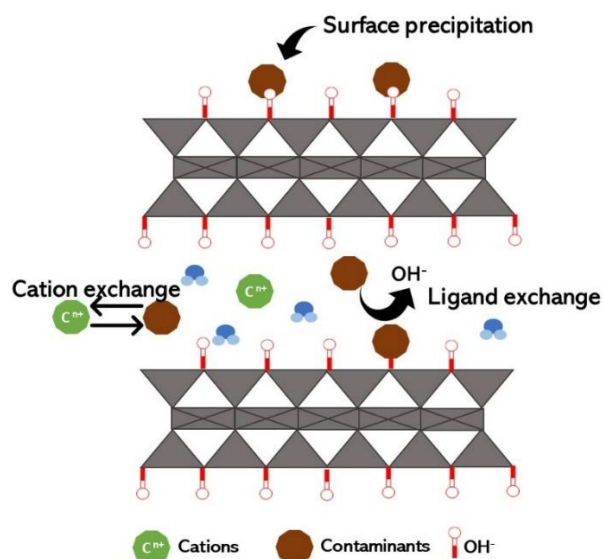


Figure 1.5 The diagram of the adsorption mechanism of clay [22].

1.2.1.3 Layered Double Hydroxides

Layered double hydroxide (LDH) is also in the group of layered inorganic materials, also called as anionic clays. The structure consists of positive-charged metal hydroxide sheets, interlayered anions and water molecules [23] (Figure 1.6). The metal hydroxide sheet is a brucite-like sheet formed by an octahedron of trivalent or divalent cations (such as Al^{3+} or Mg^{2+}) in the center and bordered with six hydroxyl groups (OH^-). The cations in the structural sheets can be replaced by isomorphic substitution; for example, Al^{3+} can replace Mg^{2+} in the upper layer. The interlayered negative charged ions are exchangeable, which is mainly their adsorption mechanism. There is also the adsorption mechanism of surface complexation and precipitation (Figure 1.7); thus, LDH has shown high sorption efficiencies for various

anionic species [24][25]. It appears to be among the best adsorbent to get rid of anionic pollutants in contaminated water.

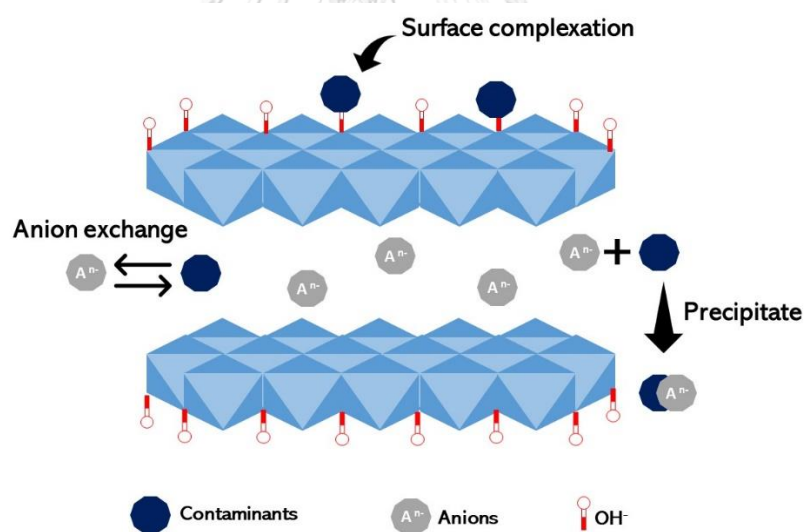
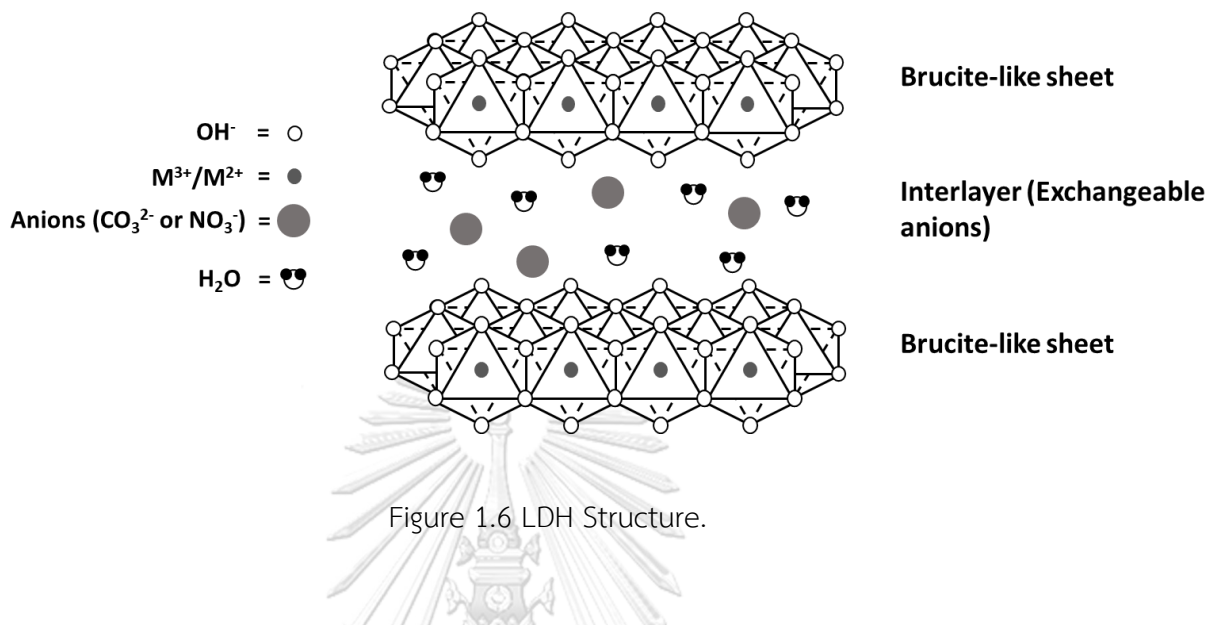


Figure 1.7 The diagram of the adsorption mechanism of LDH [25].

1.2.2 Biochar/based composites as adsorbents

Raw biochar has limited ability to adsorb pollutants from aqueous solution

for the following reasons:

1. Some functional groups derived from feedstock after pyrolysis have low activeness
2. Low surface area and pore volume for biochars were obtained at low pyrolysis temperature ($< 450^{\circ}\text{C}$)
3. Difficult separation from liquid systems due to the small size of biochar powder

Therefore, biochar modification by combining foreign materials into the biochar matrix produces a biochar composite that could lead to higher surface area and new functional properties to enhance the adsorption efficacy of biochar for a wide variety of contaminants [26].

1.2.2.1 Clay/biochar composites

Clay/biochar composites are commonly prepared by mixing biochar feedstock with clay mineral suspension, then following by pyrolysis process. The biochar serves as an excellent host to support the distribution of clay particles, such as montmorillonite, kaolinite, or bentonite, within its matrix, as a consequence, taking the advantage of superb adsorption ability of the clay minerals.

Yao et al. [27] developed a simple method to prepare clay/biochar composites for environmental applications. Montmorillonite and kaolinite/biochar composites produced from bamboo, bagasse and hickory chips were characterized by X-ray diffraction analysis. Both composites indicated well incorporation of clay

minerals into the biochar matrix. The composites revealed the crystalline phase of clay minerals along with the amorphous phase of biochar. While Scanning Electron Microscope observed the layered surfaces, imaging the similarity of the surface of the composites and pristine clays.

Kankeu E.F. et al. [28] reported the metal adsorption by bentonite/biochar composite, the composite showed the favorable adsorption towards Zn(II) as compared with Cr(VI). The Zn(II) cation was adsorbed by electrostatic with negative layers of bentonite. Meanwhile, Cr(VI) existed as the dichromate anion ($\text{Cr}_2\text{O}_7^{2-}$); therefore, the low adsorption affinity was expected.

Chen et al. [29] observed that a novel montmorillonite/bamboo biochar composite had an ability to adsorb ammonium (NH_4^+) and phosphate (PO_4^{3-}). The PO_4^{3-} adsorption affinity was more substantial than that NH_4^+ . The group proposed that the PO_4^{3-} sorption was through ionic bonding with cations presenting in the montmorillonite, while the NH_4^+ was adsorbed by cation exchange.

In addition, many researchers studied the adsorption efficiency of antibiotic contaminants on clay/biochar composites such as Norfloxacin [30], Ciprofloxacin [31], Tetracycline [32] and Oxytetracycline [33]. The primary adsorption mechanism involved chemical interaction such as hydrogen bonding, π - π interaction and ion exchange.

Therefore, using clay/composites is a better way to enhance the adsorption affinity of heavy metals, anionic and organic contaminants in an aqueous solution to treat wastewater pollutants.

1.2.2.2 LDH/biochar composites

Though biochar has shown a high adsorption efficiency for various heavy metals cations and organic contaminants, its useability by anions contaminants is limited, for example, phosphate, chromate or nitrate. Many works have reported on the modification of biochar with highly anion-effective adsorbents such as layered double hydroxides (LDHs). Anionic adsorption mechanisms using LDHs have been influenced by anion exchange or a surface complexation [25]. The synthesis approaches could be the deposition of LDHs on biochar either pre or post pyrolysis, as shown in Figure 1.8.

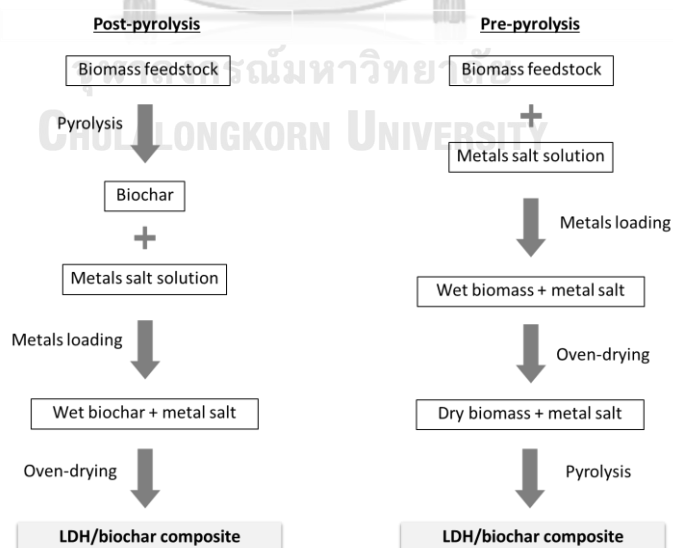


Figure 1.8 Diagrams of the post-pyrolysis and pre-pyrolysis procedures for the modification of biochar with LDH to create LDH/biochar composites.

Early investigation of LDH/biochar composites was reported by Zhang et al. [34][35]. They studied the anionic exchangeable of MgAl-LDH/cottonwood biochar composites for the adsorption of phosphate (PO_4^{3-}). The composite prepared from the post-pyrolysis method showed higher adsorption capacity than the one prepared from the pre-pyrolysis biochar.

Wang et al. [36][37] studied the adsorption of arsenate ion (AsO_4^{3-}). This work also confirmed that the post-pyrolysis NiFe/LDH-modified biochar and NiMn/LDH-modified biochar composites from the post-pyrolysis method exhibited higher adsorption capacity than the pre-pyrolysis method.

Wan et al. [38] investigated on the comparative study of different types on cation in a brucite-like sheet. The composites were the combination of Mg-Fe or Mg-Al and bamboo biochar, prepared by post-pyrolysis method. The adsorption efficiency of MgAl-LDH/bamboo biochar composite was better than that of MgFe-LDH/bamboo biochar composite.

Yang et al. [39] also studied the effect of different types of metal, including Ni-Fe, Mg-Al, and Zn-Al LDHs. The composites of these LDHs with corn stalk biochar were prepared by pre-pyrolysis method and were used for removing phosphate ions from aqueous solution. MgAl-LDH showed twice higher adsorption capacity than the others two composites.

Moreover, MgAl-LDH/biochar composites can be adsorbed organic pollutants such as dye [40][41] and heavy metal such as Pb(II) [42].

This work aims to develop a method to prepare biochar composites with clay and LDH that could remove metal cations, anionic pollutants and organic pollutants possibly presenting in contaminated water. By taking advantage of the lamellar structure and ion-exchange capabilities of clay and LDH and the porosity of biochar as substrates, the composites are supposed to perform well in various kinds of pollutants in water system. Also, they are low-cost, non-toxic and environmentally friendly.

1.3 Objectives

1. To develop the method for preparing clay/LDH/biochar nanocomposites
2. To characterize physicochemical properties of the clay/LDH/biochar nanocomposites
3. To assess their ability to remove metal ions and organic compounds
4. To apply clay-LDH-biochar nanocomposites in water treatment

CHAPTER 2 EXPERIMENTAL

2.1 Raw materials

2.1.1 Biochar

Biochar feedstocks were taken from agricultural residues waste such as bagasse and rice straw. The feedstocks were washed with deionized water and dried in an oven at 80°C for 48 hours. Then, they were pyrolyzed at 400°C [43] in a muffle furnace for 1 hour at a temperature rate of 10°C/min. The pyrolysis products were ground into fine powder of biochar.

2.1.2 Clay

Bentonite was chosen as the clay component in this research. It was purified by fractionated sedimentation method [44]. Bentonite was dispersed into deionized water in a ratio of 1:20. The mixture was stirred for 3 hours in order to suspend the clay particles. The remaining sediment was quartz impurity and was removed by centrifugation at 4000 rpm for 2 minutes. The suspended clay was dried in an oven at 80°C. The purified bentonite mainly consisted of montmorillonite clay.

2.2.1 Chemicals for MgAl-LDH

The starting materials for the synthesis of MgAl-LDH, including magnesium nitrate 6-hydrate ($\text{Mg}(\text{NO}_3)_2 \cdot 6\text{H}_2\text{O}$), aluminum nitrate 9-hydrate ($\text{Al}(\text{NO}_3)_3 \cdot 9\text{H}_2\text{O}$) and sodium hydroxide (NaOH), were purchased from PanReac AppliChem, Kemaus and Merck, respectively.

2.2 Chemicals

2.2.2 Chemicals for adsorbates

The analytical grade of Nickel chloride ($\text{NiCl}_2 \cdot 6\text{H}_2\text{O}$) and Potassium dichromate ($\text{K}_2\text{Cr}_2\text{O}_7$) used as cationic adsorbate and anionic adsorbate, were obtained from Univaris and Merck, respectively. The organic adsorbate selected 4-Nitrophenol was purchased from Sigma-Aldrich.

2.3 Preparation of clay/LDH/biochar composites

The three-component composites were synthesized by co-precipitation of MgAl-LDH in the presence of pyrolytic biochar and purified clay. The detailed procedure is described here.

The biochar from 2.1.1 was dispersed into 100 mL of deionized water under stirring for 15 minutes. The purified clay from 2.1.2 was sonicated with 100 mL of deionized water by a probe sonicator for 15 minutes. After that, clay suspension and biochar were mixed first [27]. Then $\text{Mg}(\text{NO}_3)_2 \cdot 6\text{H}_2\text{O}$ and $\text{Al}(\text{NO}_3)_3 \cdot 9\text{H}_2\text{O}$ were added into the mixture in a ratio of 4:1 [41] and the pH was adjusted to 10 using 1 M NaOH. The mixture was stirred for 24 hours. After that, the precipitates were collected and washed with deionized water and ethanol. The composite products were dried in an oven at 60°C for 24 hours. The prepared products were assigned as Clay/MgAl-LDH/bagasse biochar composite (CLB) and Clay/MgAl-LDH/rice straw biochar composite (CLR) and used as adsorbents in the adsorption process (Figure 2.1).

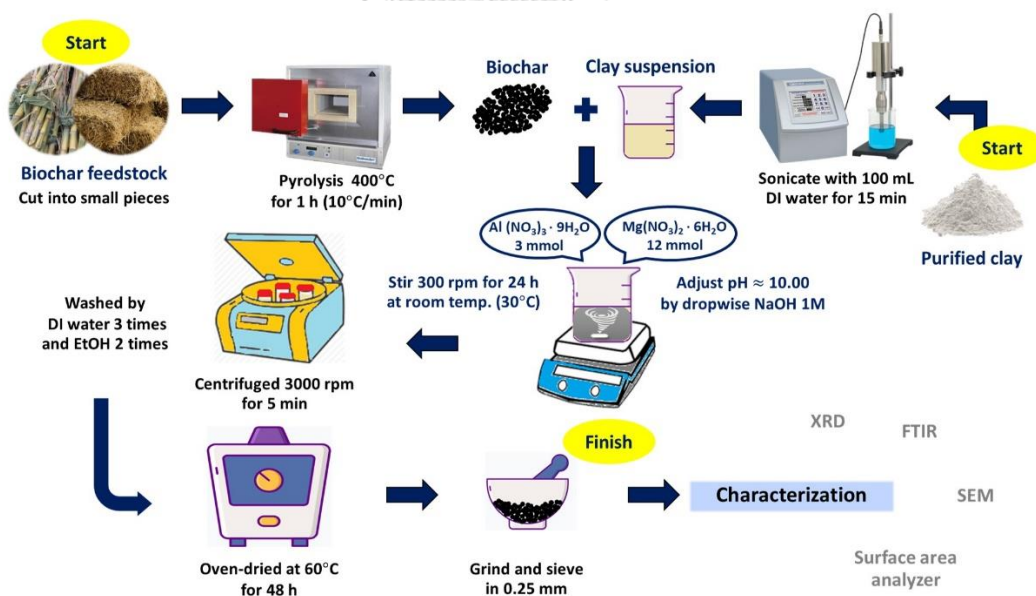


Figure 2.1 Preparation of the composites.

2.4 Characterizations

2.4.1 X-ray powder diffraction (XRD)

The structural characterization was performed using Rigaku, Smartlab 30 kV X-ray powder diffractometer. The diffractometer was equipped with a fixed monochromator and a Cu $K\alpha$ radiation source. The patterns were collected at voltage of 40 kV, an applied current of 30 mA and 2 theta (2θ) analysis angles from 3° to 70° . The divergent, scattering and receiving slits were set at 0.5° , 1° , and 0.3 mm, respectively.

2.4.2 Scanning Electron Microscopy (SEM)

The morphological surface of the composites was investigated by a JEOL IT-100 Scanning electron microscope. The samples were dispersed in ethanol, then the well-dispersed sample was dropped on copper stuff and dried at 50°C .

2.4.3 Fourier Transform Infrared Spectroscopy (FTIR)

To observed functional groups in the composites, FTIR spectra were collected at the wavenumber between 4000 to 400 cm^{-1} . The spectra were recorded as KBr pellets using a Thermo Scientific Nicolet iS50 FTIR spectrophotometer.

2.4.4 Surface area analysis

The specific surface area, pore size, and pore volume of the composites were measured by nitrogen-desorption analysis using BEL Japan BELSORP-mini II surface area analyzer. The samples were pretreated at 200°C in a vacuum using BEL Japan BELPREP-vac II for 3 hours before the measurement.

2.5 Adsorption experiments

The adsorption experiments of Ni^{2+} , CrO_4^{2-} and 4-nitrophenol were carried out in a batch system. The preliminary experiment of the fixed bed adsorption was done for the adsorption of 4-nitrophenol.

2.5.1 Batch adsorption

The condition of the batch adsorption experiments was 0.1 g adsorbent dosages, 10 mL adsorbate at varying concentration and stirring under an overhead mixer at 30 rpm for varying contact time. After that, the samples were centrifuged at 3000 rpm for 1 minute and the adsorbates were collected by using a 0.45 μ nylon syringe filter. The equilibrium concentration of the adsorbate solution was determined by Agilent 8453 UV visible spectrophotometer (Figure 2.2). The adsorption capacity (mg g^{-1}) was estimated following the equation 1;

$$Q_e = \frac{(C_i - C_e)V}{m} \quad \text{Eq. (1)}$$

Where Q_e is the adsorption capacity (mg g^{-1}); C_i is the initial concentration (mg L^{-1}); C_e is the equilibrium concentration (mg L^{-1}); V is the adsorbate volume (L) and m is the amount of adsorbent (g).

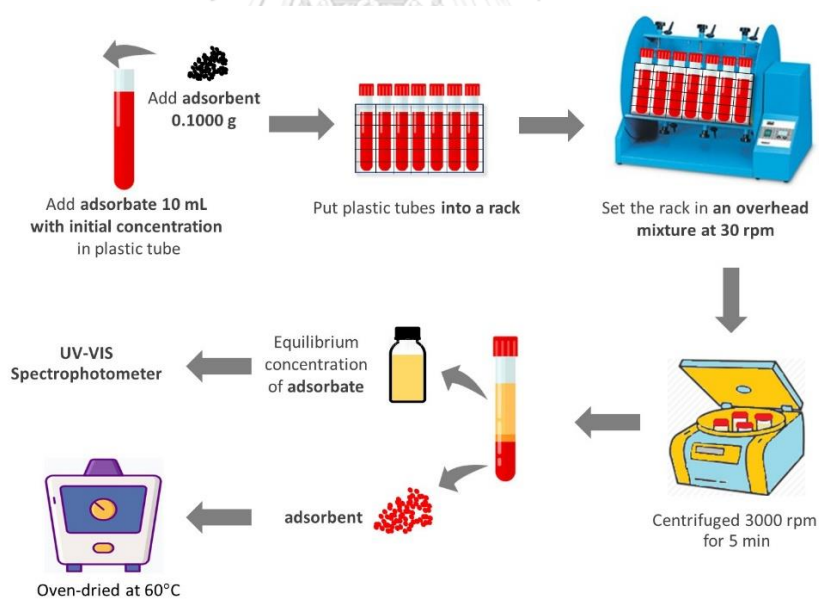


Figure 2.2 Batch adsorption.

2.5.1.1 Adsorption of Nickel(II)

Nickel solution of different concentration were diluted from the 1000 ppm NiCl_2 stock solution of $\text{pH } 7.0 \pm 0.5$.

The effect of contact time was performed by adding 0.1 g of adsorbent into 10 mL 50 mg L⁻¹ of Ni²⁺ initial concentration. The mixture was rotated at 30 rpm at room temperature for 15, 30, 60, 120 and 180 minutes.

Varying the Ni²⁺ initial concentration at 25, 50, 75, 100 and 150 mg L⁻¹ was used to study the adsorption isotherm. 0.1 g adsorbent was suspended in 10 mL Ni²⁺ solution for 120 minutes.

Ni²⁺ content at equilibrium concentration was determined by the complexation method as shown in Figure 2.3. The remaining Ni²⁺ formed the complex with dimethylglyoxime as Nickel bis-(dimethylglyoxime) [45], then its absorbance was measured by UV-visible spectrophotometer at 460 nm.

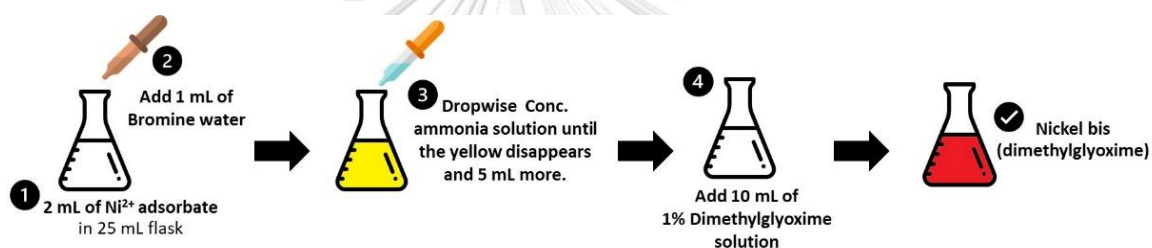


Figure 2.3 Colorimetric of Ni(II) complex with dimethylglyoxime.

2.5.1.2 Adsorption of Chromate anions

The 1000 ppm K₂Cr₂O₇ stock solution were diluted in different concentration at pH 6.5 – 7.0.

The effect of contact time was performed by adding 0.1 g of adsorbent into the 10 mL 100 mg L⁻¹ of CrO₄²⁻ initial concentration. The mixture was rotated at 30 rpm at room temperature for 0, 3, 5, 8 and 10 minutes.

Varying the CrO₄²⁻ initial concentrations at 25, 50, 75 and 100 mg L⁻¹ was used to study the adsorption isotherm. 0.1 g adsorbent was suspended in 10 mL CrO₄²⁻ solution for 5 minutes.

The pH of chromate solution was adjusted to 2.8 – 3.0 using 0.1 M H₂SO₄ before measured by a UV-visible spectrophotometer at 350 nm.

2.5.1.3 Adsorption of 4-nitrophenol

The effect of contact time was performed by adding 0.1 g of adsorbent into the 10 mL 10 mg L⁻¹ of 4-nitrophenol initial concentration. The mixture was rotated at 30 rpm at room temperature for 0.5, 3, 6, 12, 24 and 36 hours.

Varying the 4-nitrophenol initial concentrations at 2, 4, 6, 8 and 10 mg L⁻¹ was used to study the adsorption isotherm. 0.1 g adsorbent was suspended in 10 mL 4-nitrophenol solution for 24 hours.

The pH of 4-nitrophenol was adjusted to 5.5 and analyzed by UV-visible spectrophotometry at the wavelength of 318 nm [46].

2.5.2 Fixed bed adsorption

Fixed bed adsorption is the study of adsorption efficiency by a continuous flow of adsorbate through a fixed bed of an adsorbent in a column [47][48].

The experiment was conducted in a column of a plastic syringe with 9 cm height and an internal diameter of 1.5 cm. The bottom end of the column was plugged with cotton wool, and the 0.5 g adsorbent was packed into 2 cm thickness (Figure 2.4).

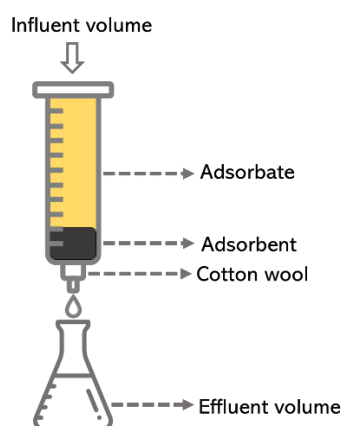


Figure 2.4 Fixed bed adsorption.

10 mL of 10 mg L⁻¹ 4-nitrophenol was passed into column. The flow rate was 0.3 mL min⁻¹. The 4-nitrophenol effluent concentration (C) was analyzed by UV-visible spectrophotometry. C/C_0 expressed the breakthrough curve as a function of the effluent volume (V), presenting the adsorption performance (Figure 2.5). From the breakthrough curve, the break point and the exhaustion point were measured when C/C_0 at lower value of 0.1 and C/C_0 approximately at 0.9, respectively.

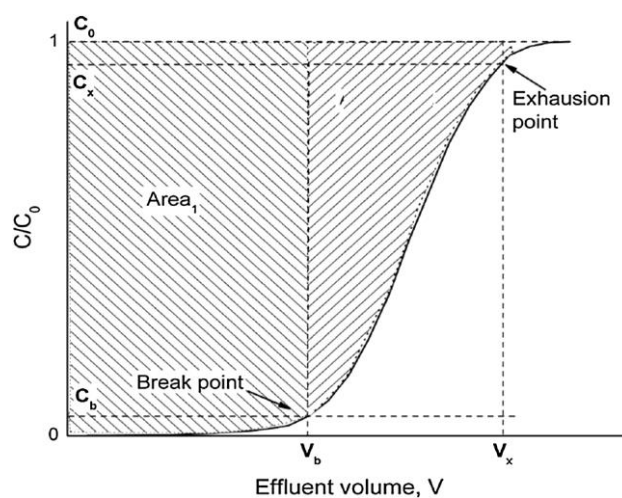


Figure 2.5 Ideal breakthrough curve [49].

CHAPTER 3 RESULTS AND DISCUSSION

3.1 Characterization of the composites

3.1.1 Structural and morphological analysis

XRD patterns (Figure 3.1) of the CLB and CLR composites show the characteristic diffraction peaks of MgAl-LDH at 11° (003) and 61° (113) [50], and those of clay at 7° (001), 20° (020) and 35° (200) [53]. The broad patterns of rice straw (R) and bagasse (B) around $15-30^\circ$ correspond to the amorphous nature of biochar. The XRD patterns of both composites, CLB and CLR, exhibit the physical combination of three components, as the highest peak of LDH (003) and the characteristic peak of clay (020) are presented at the same diffraction angles, along with the broad bump of the biochar amorphous phase. The (003) peak of LDH becomes broaden and lowers in the intensity and the (001) peak of clay disappears, suggesting that both phases are much less crystalline as compared to their pristine counterparts.

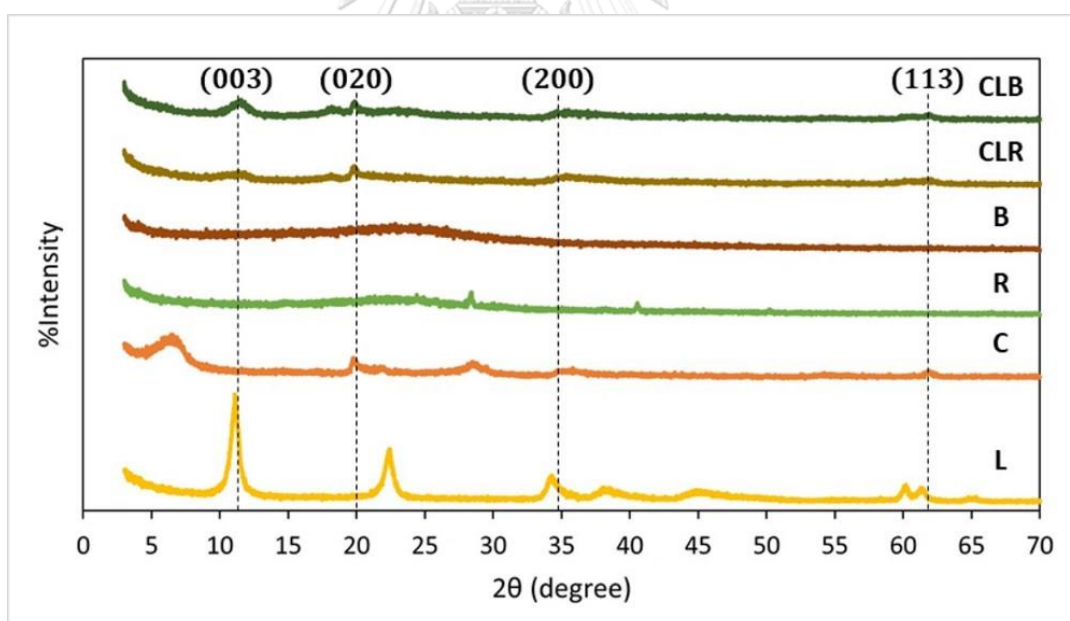


Figure 3.1 XRD patterns of CLB and CLR compared to the patterns of individual components.

(L=MgAl-LDH, C=clay, R=rice straw biochar and B=bagasse biochar)

SEM-EDS images reveal the surface morphology of the raw materials and composites. Figure 3.2 presents the surface structure of each individual components and the mapping of distinguish elements found in bagasse biochar, rice straw biochar, MgAl-LDH and clay. The SEM image of biochars display the porous network of connecting rough fibrous sheets, making it suitable as substrate matrix for the composites. Their main element is carbon (C) but silicon (Si) is also found in rice straw biochar. The particles of pristine MgAl-LDH and clay has the wide range of size distribution from a few microns to hundreds. LDH particles have smooth surface and sharp edges, while clay particles have rougher surface. The distinguish elements of MgAl-LDH and clay are Magnesium (Mg) and Silicon (Si), respectively.

Figure 3.3 and 3.4 present the morphology of the composites that could be explained as the small crystallines of LDH and clay deposited on the fibrous networks of biochar. The elemental mapping of distinguish elements shows the distribution of all three phases over every particle. This result along with the broaden XRD peaks of LDH and clay indicates that the three components mix in nanometer scale.

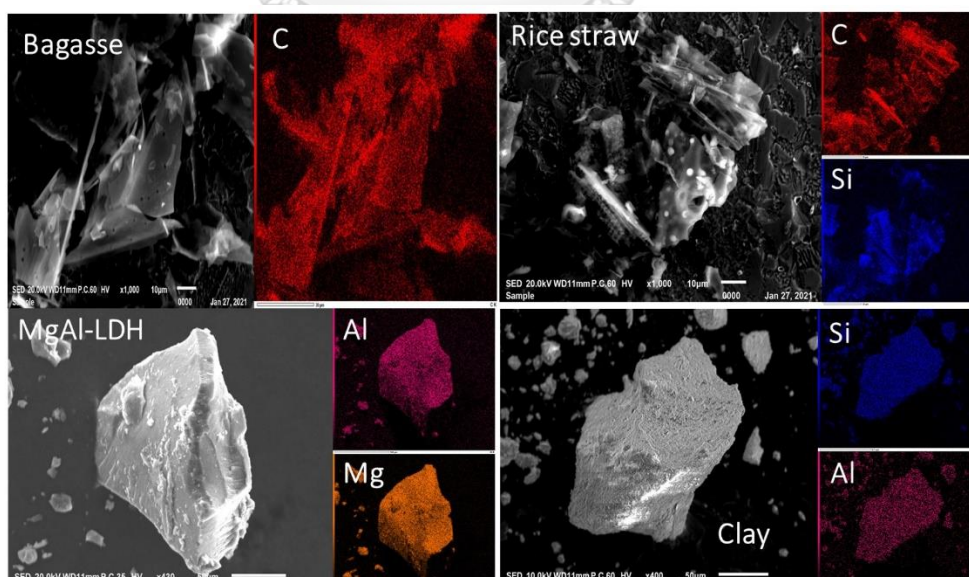


Figure 3.2 SEM images of individual components and the elemental mapping.

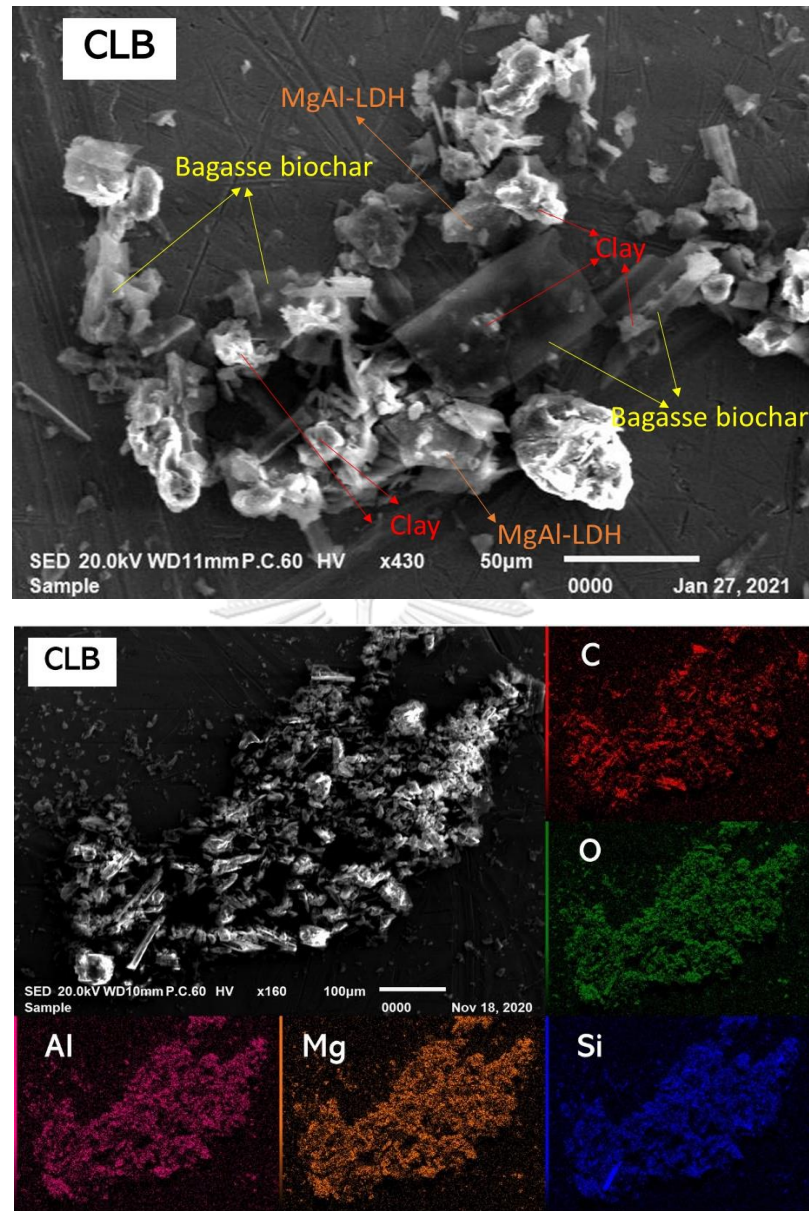


Figure 3.3 SEM images of CLB and the elemental mapping.

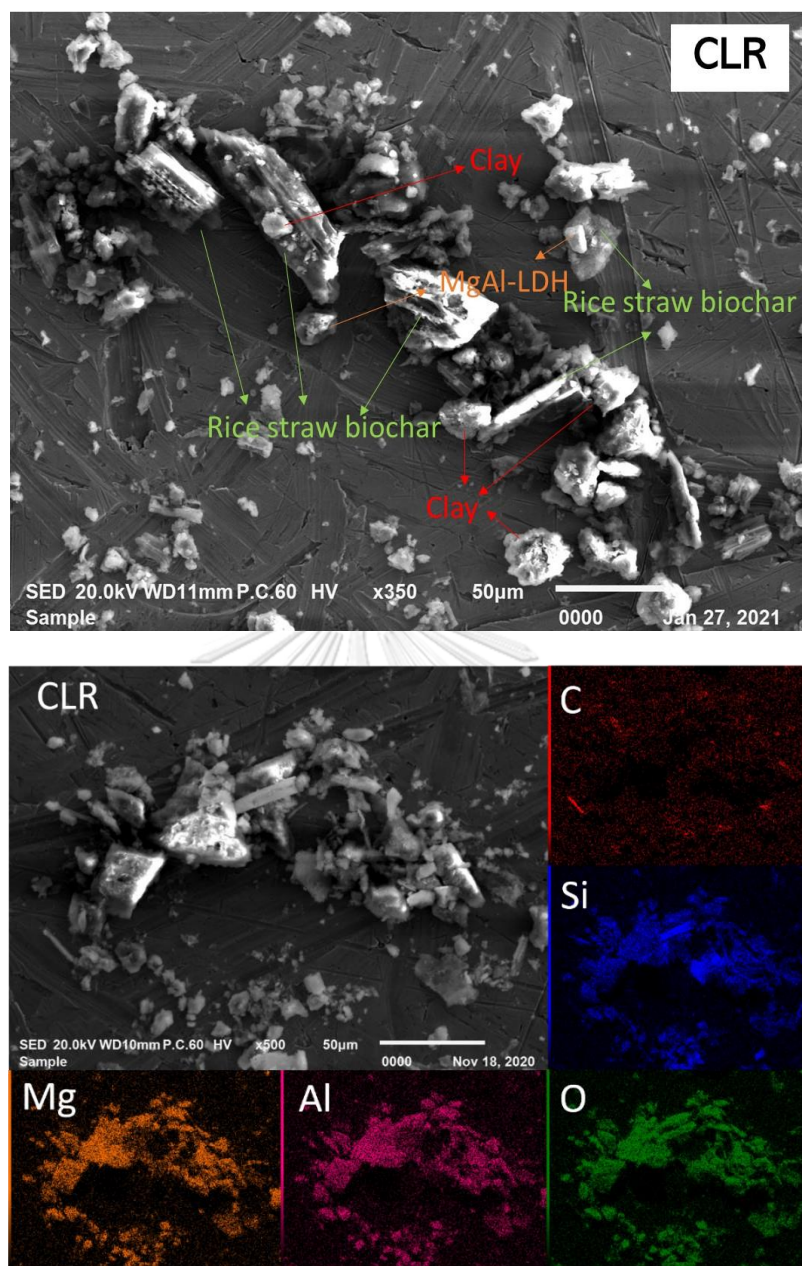


Figure 3.4 SEM images of CLR and the elemental mapping.

3.1.2 Fourier Transform Infrared analysis (FTIR)

The FTIR spectra (Figure 3.5) determine the qualitative characteristic functional groups of the composites. Their FTIR peaks of both composites match with the specific functional groups of all pristine components. The absorbance bands at 3620 and 3438 cm^{-1} indicated O-H stretching of clay (C) and MgAl-LDH (L). the peak

at 1617 cm^{-1} was C=C of both biochar. And the peak at 1384 cm^{-1} was attributed to NO_3^- in the interlayer of MgAl-LDH [42]. The FTIR peaks at lower frequency around 1000 cm^{-1} correspond to the characteristic peaks of metal-oxygen bonds (M-O and O-M-O, where M is Si, Mg and Al) such as at 1031, 915, 832, 520 and 464 cm^{-1} . All assigned peaks are summarized in Table 3.1 [29][39].

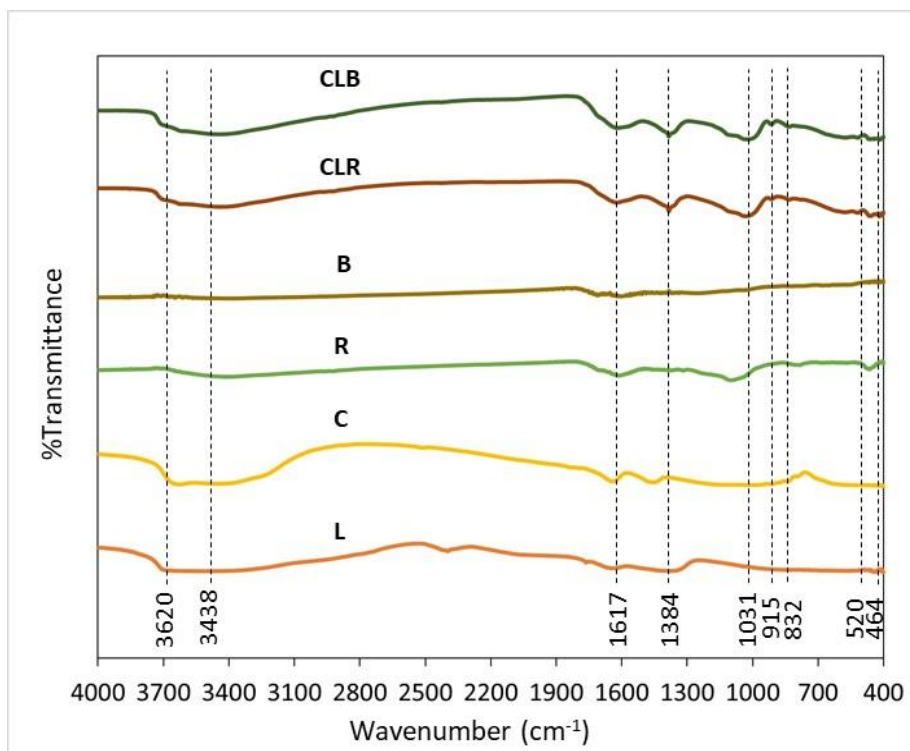


Figure 3.5 FTIR spectra of the composites (CLB and CLR) and pristine components.

Table 3.1 FTIR absorbance bands and their assigned functional groups of the composites and pristine components.

(L=MgAl-LDH, C=clay, R=rice straw biochar and B=bagasse biochar)

Absorbance band (cm ⁻¹)	Assignments	Pristine components
3620	O-H stretching bonded with Al ³⁺ cations	L and C
3438	O-H stretching (hydration)	L and C
1617	C=C stretching	B and R
1384	NO ₃ ⁻	L
1031	Si-O stretching	C and R
915	Al-Al-OH bending	C and L
832	Mg-Al-OH bending	L
520	Si-O-Al bending	C
464	Si-O-Si bending	C

3.1.3 Surface area and elemental analysis

The nitrogen adsorption-desorption of the composites (Figure 3.6) possessed type IV isotherms, indicating the mesoporous structure, according to IUPAC classification.

The obtained textural properties, including the values of surface area, total pore volume and mean pore diameter, of the composites are tabulated in Table 3.2. CLR showed a higher surface area and pore volume than CLB due to the difference in the original contents in the feedstock. The amount of lignin in rice straw and bagasse are 5% and 27%, respectively. As the feedstocks were pyrolyzed, the dehydration process of the hydroxyl group of lignin is difficult, leaving hydroxyl groups and organic residues in biochar matrix. Therefore, the bagasse biochar with the larger amount of lignin has less surface area and pore volume [52].

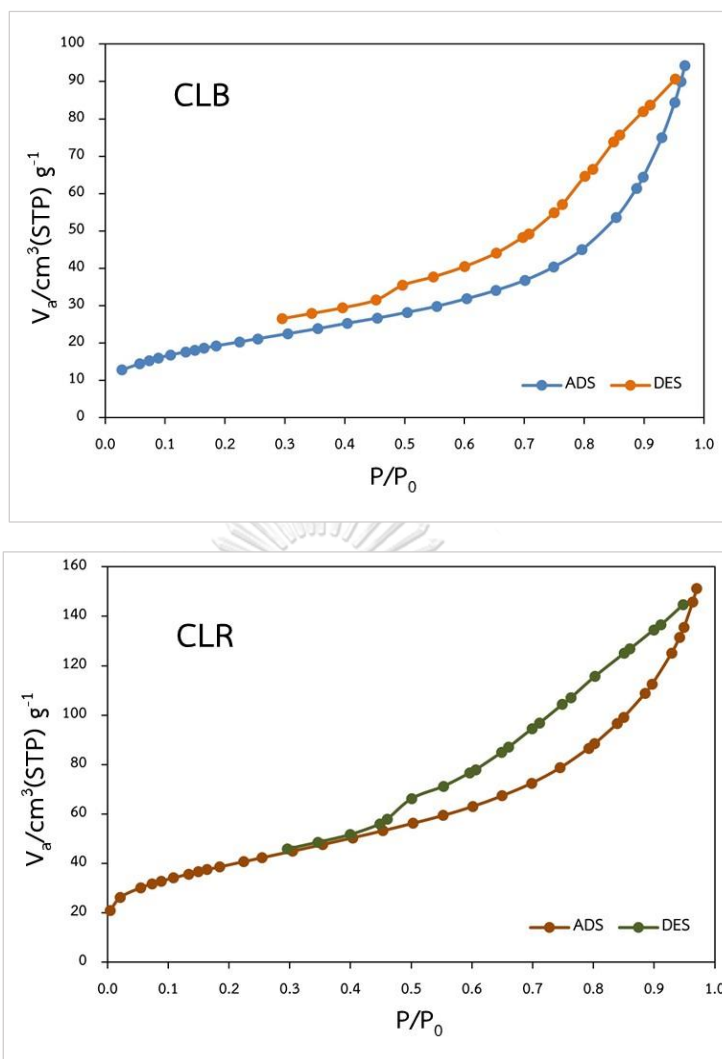


Figure 3.6 Adsorption/desorption isotherm of the composites.

Table 3.2 Textural properties of the composites.

samples	BET Specific surface area ($\text{m}^2 \text{g}^{-1}$)	Total pore volume ($\text{cm}^3 \text{g}^{-1}$)	Mean pore diameter (nm)
CLB	72.36	0.1458	8.0578
CLR	142.18	0.2339	6.5806

3.2 Adsorption studies

Adsorption studies of the composites were investigated using adsorption kinetics and adsorption isotherm to predict the mechanism of adsorption.

3.2.1 Adsorption kinetics

The kinetic adsorption studies the adsorption at various contact time, and the adsorption behavior could be regarded into the kinetic models such as the pseudo first-order model (Eq.2) and the pseudo second-order model (Eq.3).

$$\text{Pseudo first-order model; } \ln(q_e - q_t) = \ln(q_e) - k_1 t \quad \text{Eq. (2)}$$

$$\text{Pseudo second-order model; } \frac{t}{q_t} = \frac{1}{k_2 q_e^2} + \frac{t}{q_t} \quad \text{Eq. (3)}$$

Where q_t and q_e are the adsorption capacity (mg g^{-1}) at time t and at the equilibrium respectively, t is the contact time (min), k_1 is the first order rate constant (min^{-1}) and k_2 is the second order rate constant ($\text{g mg}^{-1} \text{min}^{-1}$).

The results of kinetic adsorption parameters including the type of adsorbent, adsorption capacity at equilibrium (q_e) and R^2 as the coefficient of determination, are reported in Table 3.3.

The kinetic adsorption studies of Ni(II) on CLB and CLR almost reached equilibrium at the first 15 minutes and became constant at 120 minutes. Their experiment data fit well with the pseudo second-order model as shown in Figure 3.7. The q_e of Ni^{2+} gotten from the pseudo second-order model calculation is closed that of experimental data with the R^2 of 0.9998 and 1.000 of CLB and CLR, respectively.

Similarly, in CrO_4^{2-} kinetic adsorption studies, the equilibrium was reached rapidly and the adsorption of both CLB and CLR could reach equilibrium at 5 minutes. The behavior could fit with the pseudo second-order model (Figure 3.8), with R^2 of 0.9990 and 0.9995 for CLB and CLR, respectively.

The kinetic models of the adsorption of 4-Nitrophenol are shown in Figure 3.9. Their experimental data fit well with the pseudo second-order model. The

equilibrium was reached within 24 hours with the q_e of 0.5 mg g^{-1} and 0.3 mg g^{-1} for CLB and CLR, respectively.

Table 3.3 The adsorption kinetic parameters.

Adsorbent	Adsorbate	Exp. q_e	Pseudo first order			Pseudo second order		
			Q_e	k_1	R^2	Q_e	k_2	R^2
CLB	Ni^{2+}	4.9	12.5	5.1	0.9856	5.0	7.7	0.9998
	CrO_4^{2-}	7.7	7.8	1.0	0.8956	7.6	1.9	0.9990
	4NP	0.5	1.8	0.3	0.9240	0.5	0.8	0.9911
CLR	Ni^{2+}	4.9	22.3	4.8	0.9516	5.0	7.4	1.0000
	CrO_4^{2-}	5.7	6.1	1.0	0.9200	5.7	2.2	0.9995
	4NP	0.3	8.6	0.2	0.6623	0.4	2.3	0.9983

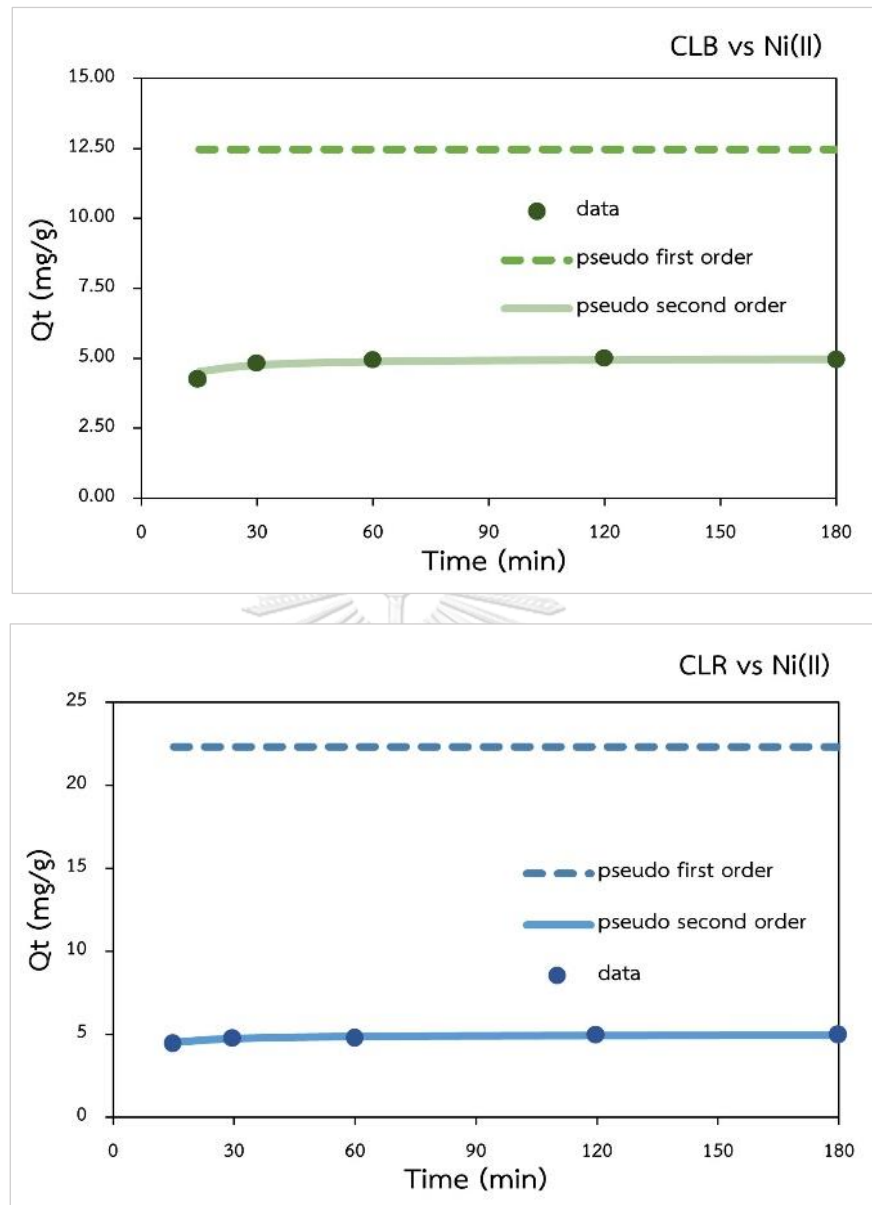


Figure 3.7 Adsorption kinetic data of Ni(II) ions.

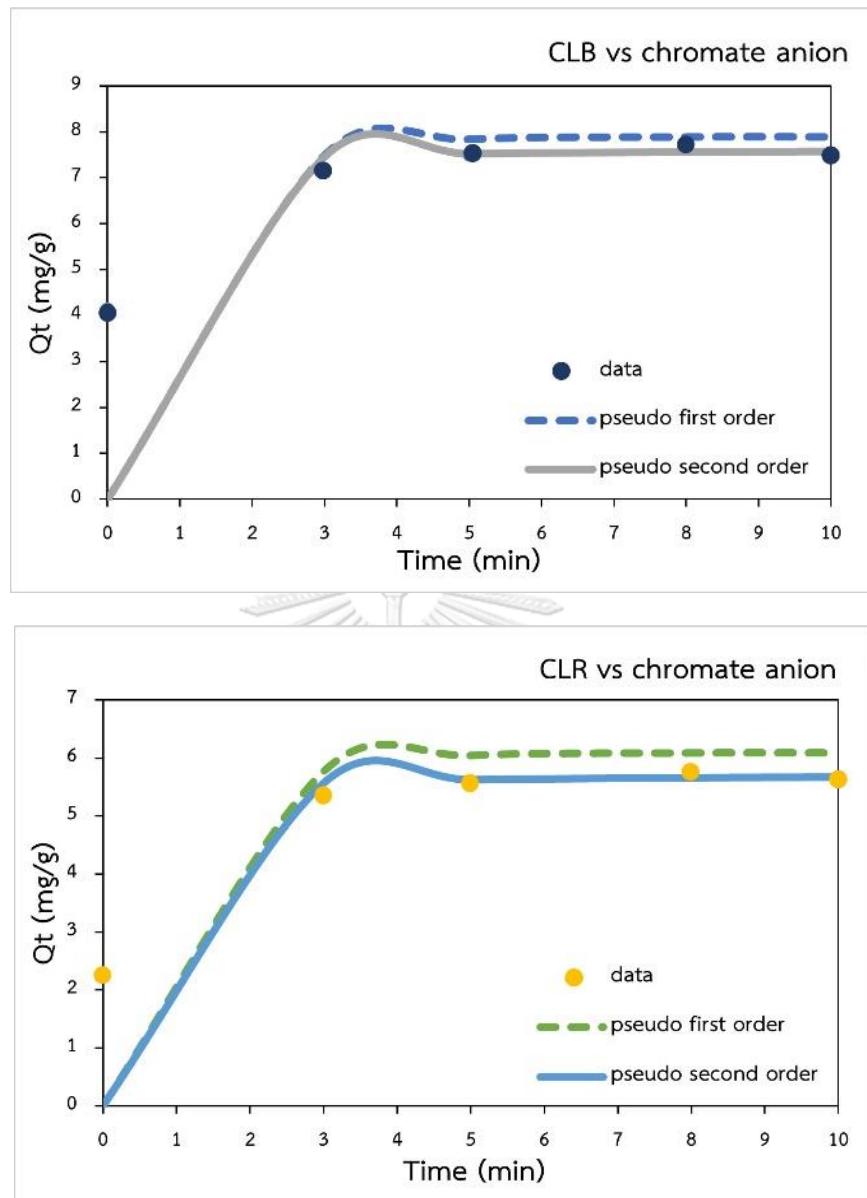


Figure 3.8 Adsorption kinetic data of CrO_4^{2-} anions.

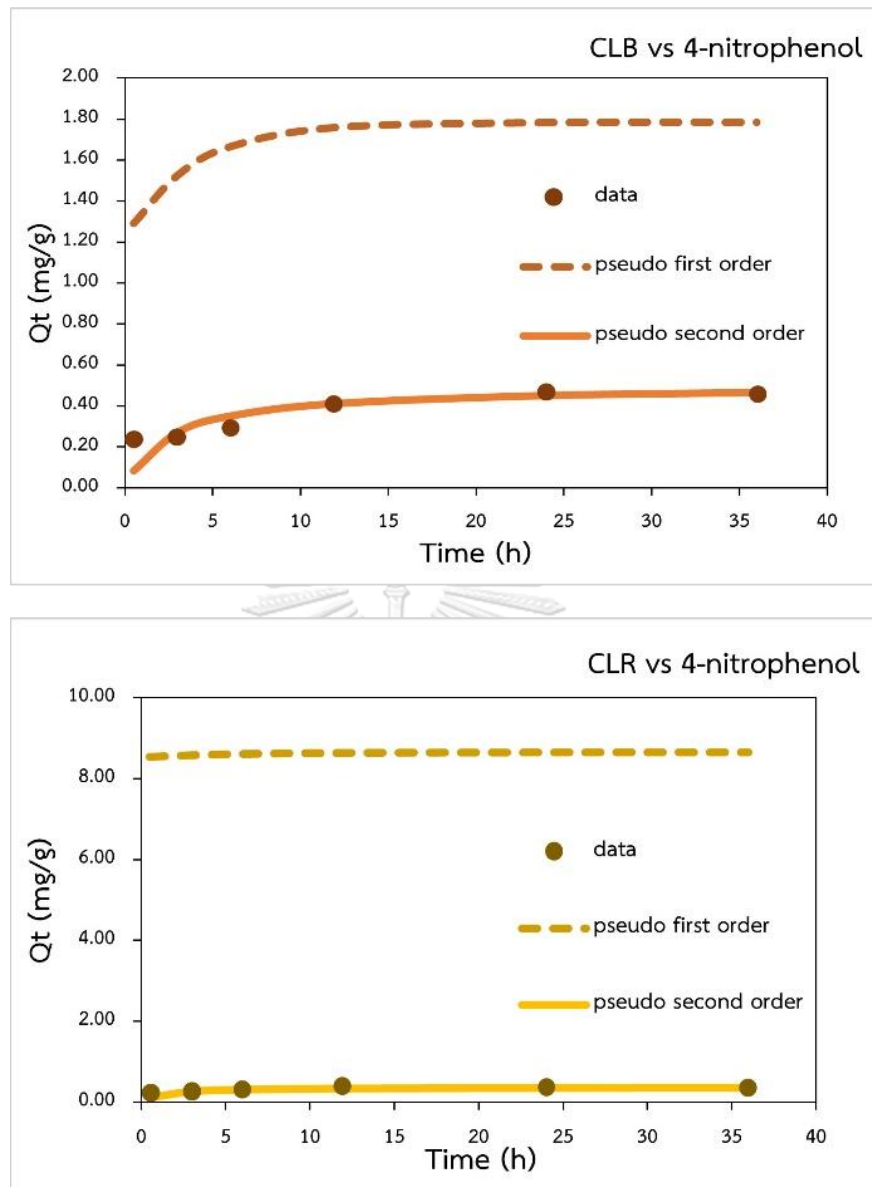


Figure 3.9 Adsorption kinetic data of 4-nitrophenol.

3.2.2 Adsorption isotherms

The adsorption behavior of the composites is investigated on the adsorption capacity at different initial concentrations. The Langmuir isotherm model and the Freundlich isotherm model are represented in Eq. 4 and 5, respectively. The Langmuir isotherm model is based on the hypothesis for the monolayer adsorption mechanism on the adsorbent surface with the regularity of energy and position. The Freundlich isotherm model relates to the assumption of the irregular multilayer adsorption on the adsorbent surface.

$$\text{Langmuir isotherm model; } \frac{C_e}{q_e} = \frac{1}{C_e Q_{\max} k_l} + \frac{1}{Q_{\max}} \quad (\text{Eq.4})$$

$$\text{Freundlich isotherm model; } \ln(q_e) = \ln(k_f) + \frac{1}{n} \ln(C_e) \quad (\text{Eq.5})$$

Where q_e is the adsorption capacity at equilibrium (mg g^{-1}), C_e is the equilibrium concentration (mg L^{-1}), Q_{\max} is the maximum adsorption capacity (mg g^{-1}), k_l and k_f are the Langmuir isotherm constant and Freundlich isotherm constant respectively, and n is the adsorption intensity. Values of $1/n$ between 0.1 and 1 indicate favorable adsorption; if $1/n$ exceeds 1, the adsorption is unfavorable.

The adsorption isotherm parameters of CLB and CLR adsorbents are reported in Table 3.4. Adsorption isotherms of Ni^{2+} and CrO_4^{2-} on both composites are suitable to be described by the Langmuir isotherm model as shown in Figure 3.10 and Figure 3.11, respectively. The Q_{\max} of CLB were 13.2 mg g^{-1} and 7.5 mg g^{-1} for the adsorption of Ni^{2+} and CrO_4^{2-} , respectively, and those of CLR were 12.7 mg g^{-1} and 6.1 mg g^{-1} .

The Freundlich isotherm model approximates the 4-nitrophenol adsorption of the composites (Figure 3.12). Adsorption intensity was obtained from the equation, determining the adsorption efficiency by the values of $1/n$. CLB and CLR displayed favorable adsorption with 0.59 and 0.55 of $1/n$ values, respectively (Table 3.4).

Table 3.4 The adsorption isotherm parameters.

Adsorbent	Adsorbate	Langmuir isotherm			Freundlich isotherm		
		Q_{\max}	k_l	R^2	$1/n$	k_f	R^2
CLB	Ni^{2+}	13.2	0.5	0.9831	0.50	3.9	0.9448
	$\text{Cr}_2\text{O}_7^{2-}$	7.5	0.4	0.9930	0.36	2.4	0.9640
	4NP	0.6	0.6	0.9896	0.59	4.9	0.9959
CLR	Ni^{2+}	12.7	0.8	0.9942	0.23	5.9	0.8850
	CrO_4^{2-}	6.1	0.2	0.9968	0.37	1.4	0.9817
	4NP	0.4	0.3	0.9815	0.55	9.3	0.9962



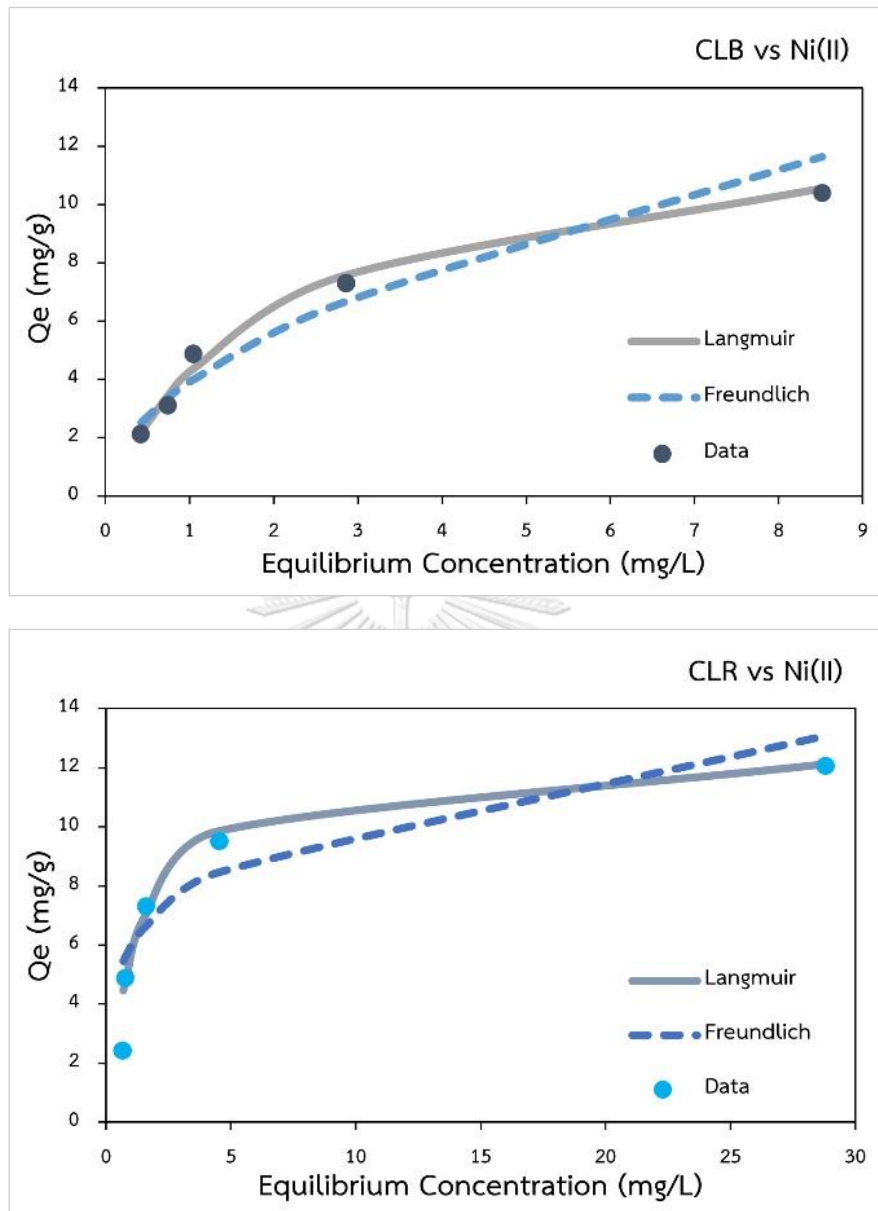


Figure 3.10 Adsorption isotherm data of Ni(II) ions.

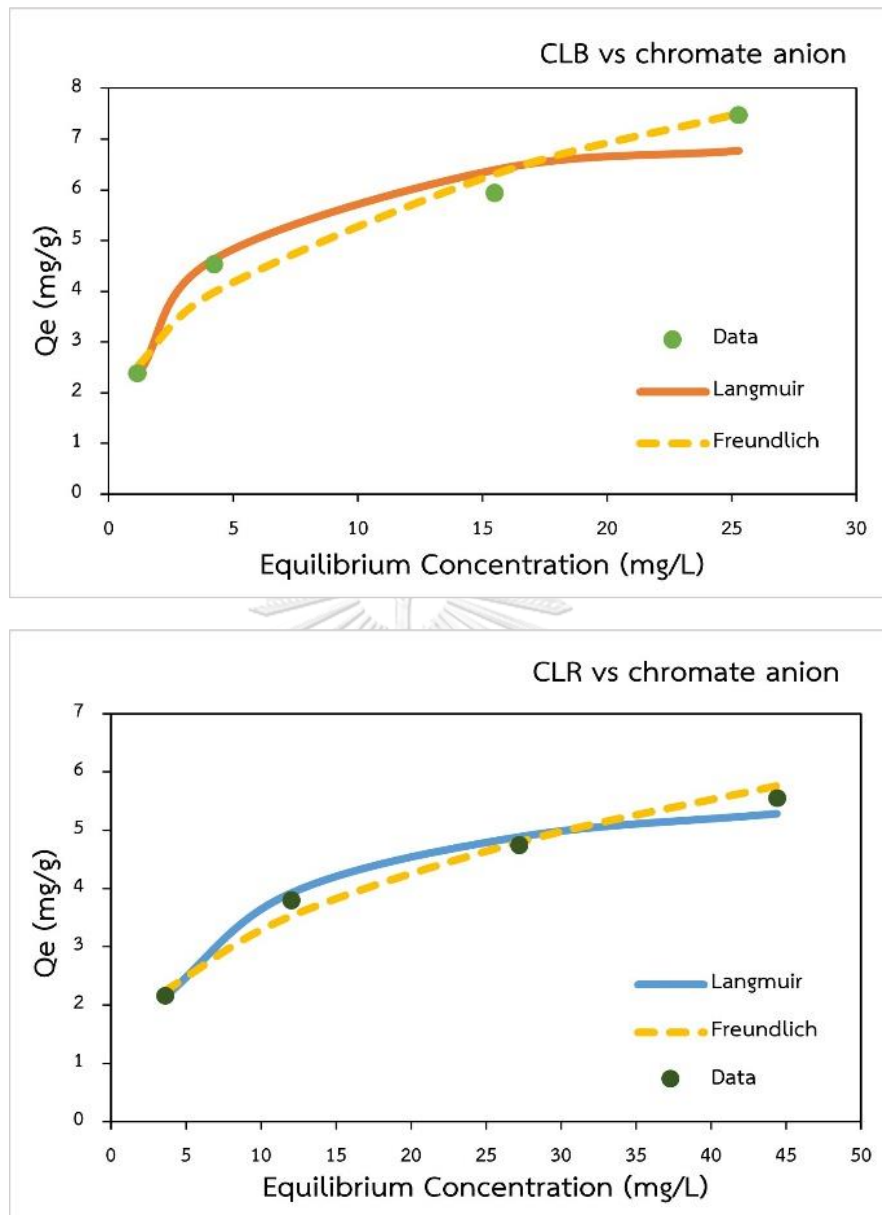


Figure 3.11 Adsorption isotherm data of CrO_4^{2-} anions.

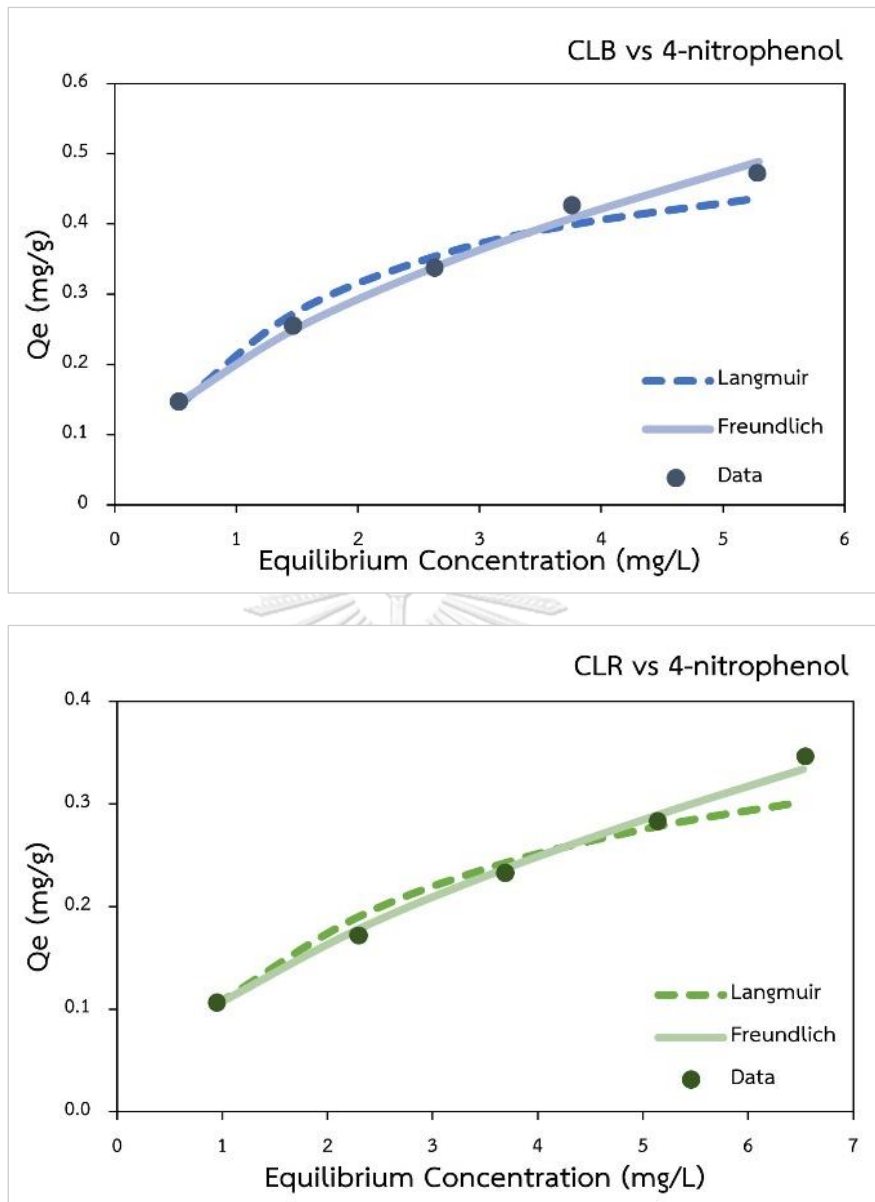


Figure 3.12 Adsorption isotherm data of 4-nitrophenol.

The adsorption capacities of the three-component composites were compared with those of pristine components in this study and also in other works, for the adsorption of Ni^{2+} in Table 3.5, the composites showed relatively high adsorption capacity compared with the pristine components. The values were competitive with the adsorption capacities of montmorillonite clay. The synthesized composites in this work were designed to have the three components in approximately the same weight; therefore, the clay active content that supposed to adsorb cation in the composites was only 1/3 of the pristine clay. The high value of adsorption capacities could due to the distribution of clay phase in composites allowing the higher approachable adsorption sites.

The adsorption capacities anionic adsorbate, CrO_4^{2-} , are summarized in Table 3.6. LDH has been reported to adsorb CrO_4^{2-} ions very well; however, both synthesized composites show very low adsorption capacity. Biochar alone could also adsorb CrO_4^{2-} ions. The reason that LDH phase in the composite cannot adsorb the anions as well as a pristine LDH could be the low crystallinity of LDH phase in the composite cannot accommodate the large amounts of anion. The low crystallinity of LDH could be interpret as the layered formation of LDH still in the early stage and the positive layered sheets could not extend into large platelets, as a result the anionic adsorption cannot strongly attached. However the distribution of LDH phase on biochar matrix allow the quick adsorption process that reach equilibrium within 5 minutes, while the values reported for the pristine LDH could take 72 hours.

Table 3.7 shows the comparison of 4-nitrophenol adsorption of the composites with the pristine components. All three phases could adsorb 4-nitrophenol, and the best one is biochar. The adsorption capacities of both composites are lower than the pure biochar, but higher than LDH and clay alone. Therefore, it seems each phase could adsorb 4-nitrophenol with its own ability.

Table 3.5 The comparison of Ni(II) adsorption capacity of the three-component composites with pristine components under given experimental conditions.

Adsorbent	Time (h)	[Ni(II)] ₀ (mg L ⁻¹)	[Dose] (g L ⁻¹)	Q _{max} (mg g ⁻¹)	References
Clay/MgAl-LDH/bagasse	2	10-200	10	13.2	This study
Clay/MgAl-LDH/rice straw	2	10-200	10	12.7	This study
Bagasse biochar	2	10-200	10	1.2	This study
Rice straw biochar	2	10-200	10	10.3	This study
Montmorillonite	2	10-200	10	15.1	This study
MgAl-LDH	2	10-200	10	95%	This study
Rice husk ash	5	100	1	4.84	[53]
Montmorillonite	3	10-50	2	11.2	[54]
Montmorillonite	N/A	50-300	20	12.9	[55]
FeMgAl-LDHs	3	10	1	1.4	[56]

Table 3.6 The comparison of CrO₄²⁻ adsorption capacity of the three-component composites with pristine components under given experimental conditions.

Adsorbent	Time (h)	[CrO ₄ ²⁻] ₀ (mg L ⁻¹)	[Dose] (g L ⁻¹)	Q _{max} (mg g ⁻¹)	References
Clay/MgAl-LDH/bagasse	5 min	25-100	10	7.5	This study
Clay/MgAl-LDH/rice straw	5 min	25-100	10	6.1	This study
Bagasse biochar	5 min	25-100	10	9.4	This study
Rice straw biochar	5 min	25-100	10	3.1	This study
Montmorillonite	5 min	25-100	10	0.3	This study
MgAl-LDH	5 min	25-100	10	833.3	This study
Bagasse sugarcane	24	10-1000	4	13.4	[57]
Rice straw	3	40-200	10	3.1	[58]
Na ⁺ Montmorillonite	2	20-100	4	0.02	[59]
MgAl-LDH	72	100-200	0.2	520.8	[60]

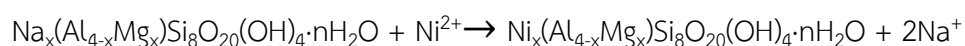
Table 3.7 The comparison of 4-nitrophenol adsorption capacity of the three-components composites with pristine components under given experimental conditions.

Adsorbent	Time (h)	[4NP] ₀ (mg L ⁻¹)	[Dose] (g L ⁻¹)	Q (mg g ⁻¹)	References
Clay/MgAl-LDH/bagasse	3	10	10	0.41	This study
Clay/MgAl-LDH/rice straw	3	10	10	0.24	This study
Bagasse biochar	3	10	10	0.99	This study
Rice straw biochar	3	10	10	0.81	This study
Montmorillonite	3	10	10	0.34	This study
MgAl-LDH	3	10	10	0.25	This study

3.2.3 Adsorption mechanism

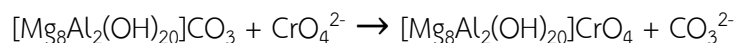
From the results above, the mechanism of adsorption are proposed here in order to understand the interactions between the adsorbents and the adsorbates. The adsorbates in this work represent various kinds of chemicals species. Ni²⁺ is the cationic adsorbate, CrO₄²⁻ is the anionic adsorbate, and 4-nitrophenol is the organic adsorbate. Each of them got adsorbed by the composites with different mechanism.

Ni²⁺ sorption on the clay/MgAl-LDH/biochar composites showed relatively high adsorption efficiency, mainly due to the negative-charge layer of clay phase. The Ni²⁺ cations were exchanged by the cations (Na⁺ or Ca²⁺) in the interlayer of clay. The cationic exchangeable mechanism could be written as:

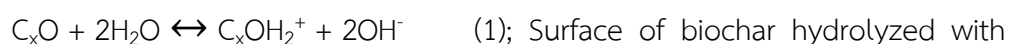


Anionic adsorbate of CrO₄²⁻ was adsorbed by MgAl-LDH and biochar. The CrO₄²⁻ anions replaced CO₃²⁻ and NO₃⁻ in the interlayer of MgAl-LDH via anion exchange. Another mechanism occurred at the surface of MgAl-LDH through

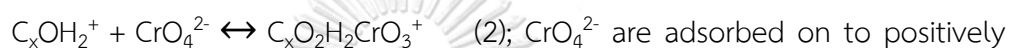
electrostatic interaction between positively charged metal hydroxide sheets with CrO_4^{2-} anions [27,62]. The cationic exchangeable mechanism could be written as:



Previous research was reported on the adsorption of CrO_4^{2-} by biochar on positively charged surface [57], which could be written as:

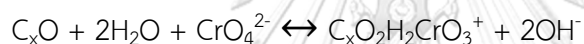


water.



charged.

Combining (1) and (2) gives:



However, in this work, the presence of LDH could overcome the amount of positive-charged biochar, it is possible that most CrO_4^{2-} anions were adsorbed by LDH phase

The adsorption mechanism of the composites for 4-nitrophenol displayed by hydrophobic site on the biochar surface, and OH^- of 4-nitrophenol exchange with OH^- on the layers of clay or MgAl-LDH via ligand exchange [46].

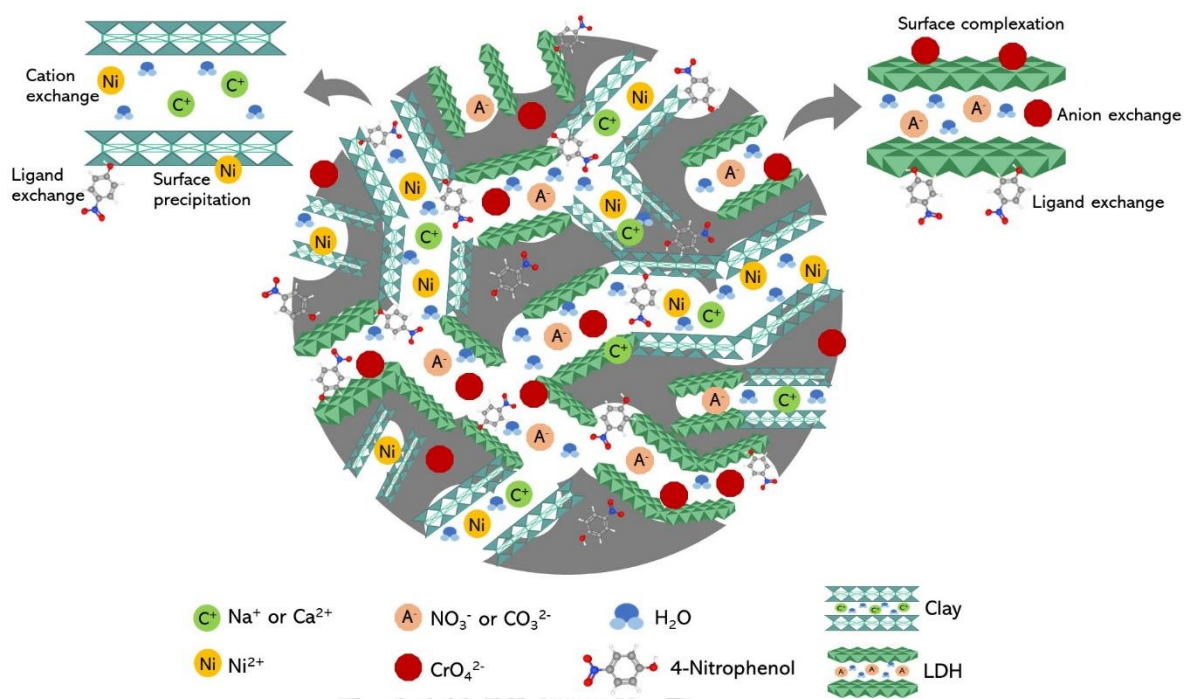


Figure 3.13 The schematic diagram of the adsorption mechanism.

3.3 Fixed bed adsorption

The study on the fixed bed adsorption of 4-nitrophenol by CLB and CLR shows the breakthrough curve with a typical S-shape as shown in Figure 3.14 and Figure 3.15, respectively. The adsorbent of 0.5 g was packed into 2 plastic syringe of 2 cm thickness, giving a gravity flow rate of 0.3 mL min^{-1} , and the initial concentration of 4-nitrophenol was 10 mg L^{-1} . The breakthrough curves of CLB and CLR show the breakthrough point at lower C_e/C_i at 0.08, corresponding to the effluent volume at 10 mL of CLR and 20 mL of CLB. The exhaustion points at C_e/C_i was 0.96, and the residue concentration near the initial concentration was found at the maximum effluent volume at 50 mL of CLR and 100 mL of CLB. The exhaustion point is the point that the adsorbent is saturated with the influent adsorbate amount [51]. The result indicates that the CLB could adsorb 4-nitrophenol more than CLR before it became saturated.

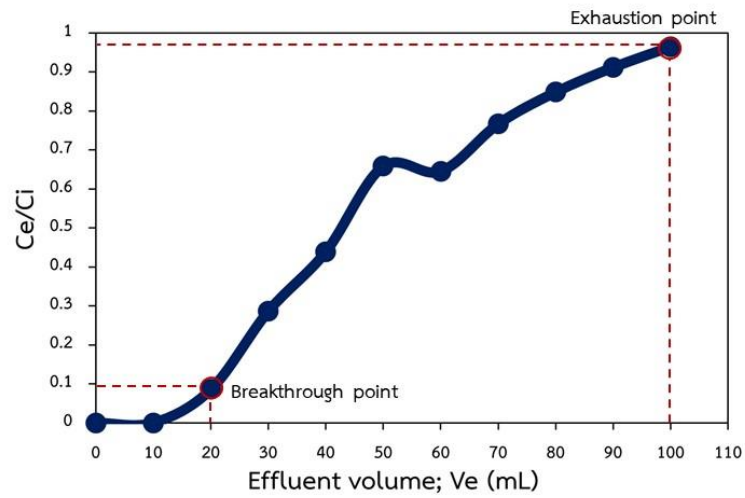


Figure 3.14 Breakthrough curve of 4-nitrophenol adsorption on CLB fixed bed column.

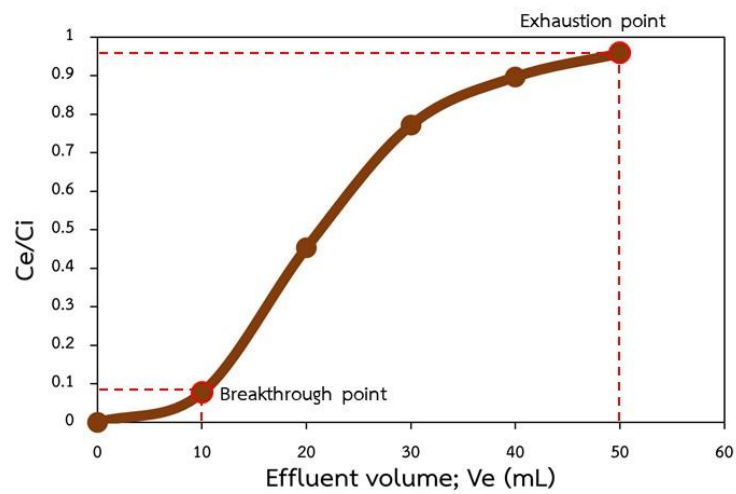


Figure 3.15 Breakthrough curve of 4-nitrophenol adsorption on CLR fixed bed column.

The cumulative adsorbed amounts calculated from Eq.6, indicates the adsorption efficiency of the composites for 4-nitrophenol in fixed bed adsorption.

$$\text{Cumulative adsorbed amount; } Q_{\text{cum}} = \sum_{V_i}^{V_e} Q = \sum_{V_i}^{V_e} \frac{(C_i - C_e)V}{m} \quad (\text{Eq.6})$$

Where Q_{cum} is the cumulative adsorbed amount (mg g^{-1}); Q is the adsorbed amount of each effluent volume (mg g^{-1}); C_i is the initial concentration (mg L^{-1}); C_e is the effluent concentration (mg L^{-1}); V is the adsorbate volume (L) and m is the mass of adsorbent (g).

From Table 3.8, the cumulative adsorbed amounts were 0.87 mg g^{-1} for CLB and 0.37 mg g^{-1} for CLR.

Table 3.8 The cumulative adsorbed amount of the composites.

(V is the volume of 4-nitrophenol of each time, V_e is the cumulative effluent volume, and Q is the adsorbed amount of each time)

Adsorbent	No.	V (mL)	V_e (mL)	Q (mg g^{-1})
CLB	1	10	10	0.20
	2	10	20	0.18
	3	10	30	0.14
	4	10	40	0.11
	5	10	50	0.07
	6	10	60	0.07
	7	10	70	0.05
	8	10	80	0.03
	9	10	90	0.02
	10	10	100	0.01
The cumulative adsorbed amount is 0.88 mg g^{-1}				
CLR	1	10	10	0.18
	2	10	20	0.11
	3	10	30	0.05
	4	10	40	0.02
	5	10	50	0.01
The cumulative adsorbed amount is 0.37 mg g^{-1}				

Although, the cumulative adsorbed amount of adsorbate is quite lower than those of the previous batch studies, this adsorbed amount values could vary in a column system depending on several parameters such as bed height, flow rate and concentrations of target adsorbates in the influent. The results from this preliminary fixed-bed experiments reveal that the composites adsorbents show a promising application in a flow-through or column system.



CHAPTER 4 CONCLUSIONS AND SUGGESTIONS

4.1 Conclusions

The ternary-component composites, CLB and CLR, were synthesized by co-precipitation of MgAl-LDH in the presence of pyrolytic biochar and purified clay. XRD, SEM-EDS and FTIR analysis confirmed the existence of the three components in the obtained composites, and suggested that clay and MgAl-LDH particles were distributed and deposited on the biochar matrix in nanometer scale.

Adsorption studies of the composites were investigated towards the various kinds of chemical contaminants species. Cations, anions and organic contaminants were represented by Ni^{2+} , CrO_4^{2-} and 4-nitrophenol, respectively. The kinetic adsorption models and the isotherm adsorption models were used to explain the adsorption capacity and behavior of the composites. Their adsorption mechanisms of each kind of the contaminants were proposed.

Ni^{2+} was adsorbed by clay phase via cation exchange in the interlayer and surface precipitation on the negative-charge layer. Meanwhile anionic contaminants of CrO_4^{2-} were mostly adsorbed by MgAl-LDH. Anions in the interlayer of MgAl-LDH exchanged with CrO_4^{2-} anions, due to their electrostatic interaction with the positive-charged metal hydroxide sheets. The mechanism of the composites for 4-nitrophenol relies on the interaction of its molecule and the hydrophobic site on the biochar.

The adsorption capacity of CLB was higher than CLR due to bagasse biochar having remaining active functional groups left in its matrix more than rice straw biochar. Hydroxyl, carbonyl and aliphatic groups have an ability to bind with contaminants by forming complexes [61]. These remaining active functional groups are the consequence of the incomplete degradation of lignin.

Moreover, the composites were explored in fixed bed adsorption system using 4-nitrophenol. The preliminary results showed that the composites could be the promising adsorbents in a column system.

4.2 Suggestions for further research

- 1) To improve the anionic adsorption capacity, the synthesis condition of LDH phase must be optimized to get larger crystallites.
- 2) More kinds of adsorbates should get tested.
- 3) Study on the reusability should be done to save cost and reduce waste.



REFERENCES



จุฬาลงกรณ์มหาวิทยาลัย
CHULALONGKORN UNIVERSITY

1. Rashid, F.; Bhatti, H.N.; Iqbal, M.; Noreen, S. "Fungal biomass composite with bentonite efficiency for nickel and zinc adsorption: A mechanistic study" *Ecol. Eng.* **2016**, *91*, 459-471.
2. Taha, A.A.; Shreadahb, M.A.; Ahmed, A.M.; Heiba, H.F. "Multi-component adsorption of Pb(II), Cd(II) and Ni(II) onto Egyptian Na-activated bentonite; equilibrium, kinetics, thermodynamics and application for seawater desalination" *J. Environ. Chem. Eng.* **2016**, *4*, 1166-1180.
3. Kara, I.; Yilmazer, D.; Akar, S.T. "Metakaolin based geopolymer as an effective adsorbent for adsorption of zinc(II) and nickel(II) ions from aqueous solutions" *Appl. Clay Sci.* **2017**, *139*, 54-63.
4. Islam, A.; Awwal, R.; Angove, M.J. "A review on nickel(II) adsorption in single and binary component systems" *J. Environ. Chem. Eng.* **2019**, *7*, 103305.
5. Al-Attar, A.M. "The Influences of Nickel Exposure on Selected Physiological Parameters and Gill Structure in the Teleost Fish, *Oreochromis niloticus*" *J. Biol. Sci.* **2007**, *7(1)*, 77-85.
6. Arif, N.; Yadav, V.; Singh, Sh.; Singh, Sw.; Ahmad, P.; Mishra, R.K.; Sharma, S.; Tripathi, D.K.; Dubey, N.K.; Chauhan, D.K. "Influence of high and low levels of plant-beneficial heavy metal ions on plant growth and development" *Front. Environ. Sci.* **2016**, *4*, 69.

7. Miretzky, P.; Cirelli, A.F. "Cr(VI) and Cr(III) removal from aqueous solution by raw and modified lignocellulosic materials: A review" *J. Hazard. Mater.* **2010**, *180*, 1-19.
8. Cotoruelo, L.M.; Marqués, M.D.; Díaz, F.J.; Mirasol, J.R.; Rodríguez, J.J.; Cordero, T. "Adsorbent ability of lignin-based activated carbons for the removal of p-nitrophenol from aqueous solutions" *Chem. Eng. J.* **2012**, *184*, 176-183.
9. Lu, Y.; Xu, Y.; Wu, Q.; Yu, H.; Zhao, Y.; Qu, J.; Huo, M.; Yuan, X. "Synthesis of Cu₂O nanocrystals/TiO₂ photonic crystal composite for efficient p-nitrophenol removal" *Colloids Surf. A Physicochem. Eng. Asp.* **2018**, *539*, 291-300.
10. Tien, C. "Chapter 2 – Adsorbents" *Introduction to Adsorption: Basics, Analysis, and Application*, Elsevier, **2019**, 7-21.
11. Qiu, Y.; Zheng, Z.; Zhou, Z.; Sheng, G.D. "Effectiveness and mechanisms of dye adsorption on a straw-based biochar" *Bioresour. Technol.* **2009**, *100*, 5348-5351.
12. Tong, X.J.; Li, J.Y.; Yuan, J.H.; Xu, R.K. "Adsorption of Cu(II) by biochars generated from three crop straws" *Chem. Eng. J.* **2011**, *172*, 828-834.
13. Kong, H.; He, J.; Gao, Y.; Wu, H.; Zhu, X. "Cosorption of phenanthrene and mercury(II) from aqueous solution by soybean stalk-based biochar" *J. Agric. Food Chem.* **2011**, *59*, 12116-12123.
14. Lima, I.M.; Boateng, A.A.; Klasson, K.T. "Physicochemical and adsorptive properties of fast-pyrolysis biochars and their steam activated counterparts" *J. Chem. Technol. Biotechnol.* **2010**, *85*, 1515-1521.
15. Yao, Y.; Gao, B.; Inyang, M.; Zimmerman, A.R.; Cao, X.; Pullammanappallil, P. "Removal of phosphate from aqueous solution by biochar derived from

- anaerobically digested sugar beet tailings” *J. Hazard. Mater.* **2011**, *190*, 501-507.
16. Chintala, R.; Mollinedo, J.; Schumacher, T.E.; Papiernik, S.K.; Malo, D.D.; Clay, D.E. “Nitrate sorption and desorption in biochars from fast pyrolysis” *Microporous Mesoporous Mater.* **2013**, *179*, 250-257.
17. Sizmur, T.; Fresno, T.; Akgül, G; Frost, H; Jiménez, E.M. “Biochar modification to enhance sorption of inorganics from water” *Bioresour. Technol.* **2017**, *246*, 34-47.
18. Galton-Fenzi, B.K. “The Clay Mineral-Structure”
http://www.groundwaterresearch.com.au/reference_files/hydrology_and_the_clay_minerals/structure.htm (accessed July 14, 2021)
19. Gurses, A.; Dogar, C.; Yalcin, M.; Acikyildiz, M.; Bayrak, R.; Karaca, S. “The adsorption kinetics of the cationic dye, methylene blue, onto clay” *J. Hazard. Mater.* **2006**, *131*, 217-228.
20. Otunola, B.O.; Ololade, O.O. “A review on the application of clay minerals as heavy metal adsorbents for remediation purposes” *Environ. Technol. Innov.* **2020**, *18*, 100692.
21. Awad, A.M.; Shaikh, S.M.R.; Jalab, R.; Gulied, M.H.; Nasser, M.S.; Benamor, A.; Adham, S. “Adsorption of organic pollutants by natural and modified clays: A comprehensive review” *Sep. Purif. Technol.* **2019**, *228*, 115719.

22. Zhu, R.; Chen, Q.; Zhou, Q.; Xi, Y.; Zhu, J.; He, H. "Adsorbents based on montmorillonite for contaminant removal from water: A review" *Appl. Clay Sci.* **2016**, *123*, 239-258.
23. Mishra, G.; Dash, B.; Pandey, S. "Layered double hydroxides: A brief review from fundamentals to application as evolving biomaterials: A review" *Appl. Clay Sci.* **2018**, *153*, 172-186.
24. Goh, K.H.; Lim, T.T.; Dong, Z. "Application of layered double hydroxides for removal of oxyanions: A review" *Water Res.* **2008**, *42*, 1343-1368.
25. Zhang, R.; Ai, Y.; Lu, Z. "Application of multifunctional layered double hydroxides for removing environmental pollutants: Recent experimental and theoretical progress" *J. Environ. Chem. Eng.* **2020**, *8*, 103908.
26. Karakoyun, N.; Kubilay, S.; Aktas, N.; Turhan, O.; Kasimoglu, M.; Yilmaz, S. "Hydrogel-biochar composites for effective organic contaminant removal from aqueous media" *Desalination.* **2011**, *280*, 319-325.
27. Yao, Y.; Gao, B.; Fang, J.; Zhang, M.; Chen, H.; Zhou, Y.; Creamer, A.E.; Sun, Y.; Yang, L. "Characterization and environmental application of clay-biochar composites" *Chem. Eng. J.* **2014**, *242*, 136-143.
28. Kankeu, E.F.; Waanders, F.B.; Steyn, F.W. "The preparation and characterization of clay-biochar composites for the removal of metal pollutants" <http://www.researchgate.net/publication/286018797> (accessed January 21,2020)

29. Chen, L.; Chen, X.L.; Zhou, C.H.; Yang, H.M.; Ji, S.F.; Tong, D.S.; Zhong, Z.K.; Yu, W.H.; Chu, M.Q. “Environmental-friendly montmorillonite-biochar composites: Facile production and tunable adsorption-release of ammonium and phosphate” *J. Clean. Prod.* **2017**, *156*, 648-659.
30. Li, Y.; Wang, Z.; Xie, X.; Zhu, J.; Li, R.; Qin, T. “Removal of Norfloxacin from aqueous solution by clay-biochar composite prepared from potato stem and natural attapulgite” *Colloids Surf. A Physicochem. Eng. Asp.* **2017**, *514*, 126-136.
31. Ashiq, A.; Sarkar, B.; Adassoriya, N.; Walpita, J.; Rajapaksha, A.U.; Ok, Y.S.; Vithanage, M. “Sorption process of municipal solid waste biochar-montmorillonite composite for ciprofloxacin removal in aqueous media” *Chemosphere.* **2019**, *236*, 124384.
32. Premarathna, K.S.D.; Rajapaksha, A.U.; Adassoriya, N.; Sarkar, B.; Sirimuthu, N.M.S.; Cooray, A.; Ok, Y.S.; Vithanage, M. “Clay-biochar composites for sorptive removal of tetracycline antibiotic in aqueous media” *J. Environ. Manage.* **2019**, *238*, 315-322.
33. Liang, G.; Wang, Z.; Yang, X.; Qin, T.; Xie, X.; Zhao, J.; Li, S. “Efficient removal of oxytetracycline from aqueous solution using magnetic montmorillonite-biochar composite prepared by one step pyrolysis” *J. Environ. Manage.* **2019**, *695*, 133800.

34. Zhang, M.; Gao, B.; Yao, Y.; Inyang, M. "Phosphate removal ability of biochar/MgAl-LDH ultra-fine composites prepared by liquid-phase deposition" *Chemosphere*. **2013**, *92*, 1042-1047.
35. Zhang, M; Gao, B.; Fang, J.; Creamer, A.E.; Ullman, J.L. "Self-assembly of needle-like layered double hydroxide (LDH) nanocrystals on hydrochar: characterization and phosphate removal ability" *RSC Adv*. **2014**, *4*, 28171.
36. Wang, S.; Gao, B.; Li, Y.; Zimmerman, A.R.; Cao, X. "Sorption of arsenic onto Ni/Fe layered double hydroxide (LDH)-biochar composites" *RSC Adv*. **2016**, *6*, 17792.
37. Wang, S.; Gao, B.; Li, Y. "Enhanced arsenic removal by biochar modified with nickel (Ni) and manganese (Mn) oxyhydroxides" *J. Ind. Eng. Chem*. **2016**, *37*, 361-365.
38. Wan, S.; Wang, S.; Li, Y.; Gao, B. "Functionalizing biochar with Mg-Al and Mg-Fe layered double hydroxides for removal of phosphate from aqueous solutions" *J. Ind. Eng. Chem*. **2017**, *47*, 246-253.
39. Yang, F.; Zhang, S.; Sun, Y.; Tsang, D.C.W.; Cheng, K.; Ok, Y.S. "Assembling biochar with various layered double hydroxides for enhancement of phosphorus recovery" *J. Hazard. Mater*. **2019**, *365*, 665-673.
40. Tan, X.; Liu, Y.; Gu, Y.; Liu, S.; Zeng, G.; Cai, X.; Hu, X.; Wang, H.; Liu, S.; Jiang, L. "Biochar pyrolyzed from MgAl-layered double hydroxides pre-coated remie

- biomass (*Boehmeria nivea* (L.) Gaud.): Characterization and application for crystal violet removal” *J. Environ. Manage.* **2016**, *184*, 85-93.
41. Meili, L.; Lins, P.V.; Zanta, C.L.P.S.; Soletti, J.I.; Ribeiro, L.M.O.; Dornelas, C.B.; Silva, T.L.; Vieira, M.G.A. “MgAl-LDH/Biochar composites for methylene blue removal by adsorption” *Appl. Clay Sci.* **2019**, *168*, 11-20.
42. Wang, C.; Wang, H. “Pb(II) sorption from aqueous solution by novel biochar loaded with nano-particles” *Chemosphere.* **2018**, *192*, 1-4.
43. Chen, L.; Chen, X.L.; Zhou, C.H.; Yang, H.M.; Ji, S.F.; Tong, D.S.; Zhong, Z.K.; Yu, W.H.; Chu, M.Q. “Environmental-friendly montmorillonite-biochar composites: Facile production and tunable adsorption-release of ammonium and phosphate” *J. Clean. Prod.* **2017**, *156*, 648-659.
44. Kanjanaboomalert, T. Synthesis and Catalytic Activity in Alkylation Reaction of Iron and Gallium-dopes Iron Oxides Pillared Clays, M.Sc. Thesis, Department of Chemistry, Chulalongkorn University, Bangkok, **2004**.
45. Mitchell, A.M.; Mellon, M.G. “Colorimetric Determination of Nickel with Dimethylglyoxime” *Ind. Eng. Chem. Res.* **1945**, *17*, 6, 380-382.
46. Wang, P.; Tang, L.; Wei, X.; Zeng, G.; Zhou, Y.; Deng, Y.; Wang, J.; Xie, Z.; Fang, W. “Synthesis and application of iron and zinc doped biochar for removal of *p*-nitrophenol in wastewater and assessment of the influence of co-existed Pb(II)” *Appl. Surf. Sci.* **2017**, *392*, 391-401.

47. Marzbali, M.H.; Esmaili, M. "Fixed bed adsorption of tetracycline on a mesoporous activated carbon: Experimental study and neuro-fuzzy modeling" *J. Appl. Res. Technol.* **2017**, *15*, 454-463.
48. Du, Z.; Zheng, T.; Wang, P. "Experimental and modelling studies on fixed bed adsorption for Cu(II) removal from aqueous solution by carboxyl modified jute fiber" *Powder Technol.* **2018**, *338*, 952-959.
49. Patel, H. "Fixed-bed column adsorption study: a comprehensive review" *Appl. water sci.* **2019**, *9*, 45.
50. Li, R.; Wang, J.J.; Zhou, B.; Awasthi, MK; Ali, A.; Zhang, Z.; Gaston, L.A.; Lahori, AH; Mahar, A. "Enhancing phosphate adsorption by Mg/Al layered double hydroxide functionalized biochar with different Mg/Al ratios" *Sci. Total Environ.* **2016**, *559*, 121-129.
51. Shahwan, T.; Erten, H.N. "Sorption studies of Cs⁺, Ba²⁺, and Co²⁺ ions on bentonite using radiotracer, ToF-SIMS, and XRD techniques" *Radiochim. Acta.* **2001**, *89*, 799-804.
52. Miretzky P.; Cirelli A.F. "Cr (VI) and Cr (III) removal from aqueous solution by raw and modified lignocellulosic materials: A review" *J. of Hazard. Mater.* **2010**, *180*, 1-19.
53. Srivastava, V.C.; Mall, I.D.; Mishra, I.M. "Competitive adsorption of cadmium(II) and nickel(II) metal ions from aqueous solution onto rice husk ash" *Chem. Eng. Process.: Process Intensif.* **2009**, *48*, 370-379.

54. Gupta, S.S.; Bhattacharyya, K.G. "Immobilization of Pb(II), Cd(II) and Ni(II) ions on kaolinite and montmorillonite surfaces from aqueous medium" *J. Environ. Manage.* **2008**, *87*, 46-58.
55. Ijagbemi, C.O.; Baek, M.H.; Kim, D.S. "Montmorillonite surface properties and sorption characteristics for heavy metal removal from aqueous solutions" *J. Hazard. Mater.* **2009**, *166*, 538-546.
56. Jawad, A.; Peng, L.; Liao, Z.; Zhou, Z.; Shahzad, A.; Ifthikar, J.; Zhao, M.; Chen, Z.; Chen, Z. "Selective removal of heavy metals by hydrotalcites as adsorbents in diverse wastewater: Different intercalated anions with different mechanisms" *J. Clean. Prod.* **2019**, *211*, 1112-1126.
57. Sharma, D.C.; Forster, C.F. "A preliminary examination into the adsorption of hexavalent chromium using low-cost adsorbents" *Bioresour. Technol.* **1994**, *47*, 257-264.
58. Gao, H.; Liu, Y.; Zeng, G.; Xu, W.; Li, T.; Xia, W. "Characterization of Cr(VI) removal from aqueous solutions by a surplus agricultural waste-Rice straw" *J. Hazard. Mater.* **2008**, *150*, 446-452.
59. Wang, G.; Hua, Y.; Su, X.; Komarneni, S.; Ma, S.; Wang, Y. "Cr(VI) adsorption by montmorillonite nanocomposites" *Appl. Clay Sci.* **2016**, *124-125*, 111-118.
60. Lu, L.; Li, J.; Ng, D.H.L.; Yang, P.; Song, P.; Zuo, M. "Synthesis of novel hierarchically porous Fe₃O₄@MgAl-LDH magnetic microspheres and its superb

adsorption properties of dye from water” *J. Ind. Eng. Chem.* **2017**, *46*, 315-323.

61. Demirbas, A. “Heavy metal adsorption onto agro-based waste materials: A review” *J. Hazard. Mater.* **2008**, *157*, 220-229.



VITA

NAME Sutasinee Sutthiklub

DATE OF BIRTH 17 October 1995

PLACE OF BIRTH Bangkok, Thailand

INSTITUTIONS ATTENDED B.SC., Geoscience, Mahidol University, Nakhon Pathom, Thailand, December 2018

HOME ADDRESS 40/717 Nuanchan Soi 14 Yak 3, Nuanchan Road, Nuanchan Sub-district, Bueng Kum District, Bangkok, Thailand, 10230

